Targeting Dormant Disseminated Tumor Cells and their Permissive Niche by Pro-Resolving Mediators Derived from Resolution-Phase Macrophages.

Odelya Gilon-Zaltsman
University of Haifa
Keren Weidenfeld
University of Haifa
Hadeel Samara
University of Haifa
Yonatan Feuermann
University of Haifa
Shira Michaeli-Ashkenasi
University of Haifa
Sagie Schif-Zuck
University of Haifa https://orcid.org/0000-0001-5415-9488
Palle Von Huth
University of Haifa
Sergei Butenko
University of California Irvine https://orcid.org/0000-0001-9759-9897
Simaan Assi
University of Haifa
Edmond Sabo
Carmel medical center
Amiram Ariel
University of Haifa https://orcid.org/0000-0002-7469-5728
Dalit Barkan (dalitbrk@gmail.com)
University of Haifa

Article

Keywords:

Posted Date: September 14th, 2023

DOI: https://doi.org/10.21203/rs.3.rs-3351611/v1

Additional Declarations: Yes there is potential Competing Interest. The research was partly supported by ResCure Pharma until 2017. DB and AA served as scientific consultants at ResCure Pharma until 2017. YF was the scientific manager at ResCure Pharma until 2017. Patent application covering part of the manuscript was awarded : Barkan D, Gilon O, Schif-Zuck S and Ariel A. CD11blow macrophages and conditioned media thereof for treating cancer and /or fibrosis. Patent application No. WO2014102799A1 https://patents.google.com/patent/WO2014102799A1/en. DB is a scientific consultant to VuJaDe Sciences.

Targeting Dormant Disseminated Tumor Cells and their Permissive Niche by Pro-Resolving Mediators Derived from Resolution-Phase Macrophages.

Odelya Gilon-Zaltsman [1#], Keren Weidenfeld-Barenboim [1#], Hadeel Samara, Yonatan Feuermann[1], Shira Michaeli-Ashkenasi [1], Sagie Schif-Zuck[1], Palle Von Huth[2], Sergei Butenko[1], Simaan Assi[1], Edmond Sabo[3], Amiram Ariel[1] and Dalit Barkan[1*]

[1]Department of Human Biology, University of Haifa, Haifa, Israel.

[2] Bioimaging Unit, University of Haifa, Haifa, Israel.

[3]Department of Pathology, Carmel Hospital, Israel

[#] Contributed equally

Running title: Inhibiting Metastatic Outgrowth of Dormant Disseminated Tumor Cells by Soluble Mediators of Resolution-Phase Macrophages.

*Corresponding Author: Dalit Barkan, Department of Human Biology, Faculty of Natural Sciences, University of Haifa, Haifa, Israel 31905. E-mail: dalitbrk@gmail.com. Fax: 972-48288763, Tel: 972-48288789.

Abstract

Metastatic breast cancer can recur years after initial treatments and arise from quiescent disseminated tumor cells (QDTC). To date there are no treatments to target QDTCs. Previously, the fibrotic-like niche (FLN) enriched with Type I collagen (Col-I) was shown to be required for the switch of QDTC to overt metastases. Here, we examined whether reinstating resolution of inflammation, by using soluble mediators secreted by *ex-vivo* generated pro-resolving CD11b^{low} macrophages (CM-Mres), will prevent FLN establishment and in turn hinder QDTC outgrowth. Our findings indicate that CM-Mres promoted immune silencing at the metastatic site as part of the resolution process and inhibited the FLN resulting in the inhibition of the metastatic outgrowth *in vitro* and *in vivo*. This was due to inhibition of fibroblasts to myofibroblasts differentiation independent of TGFβ1 canonical signaling and the abolishment of Col-I expression. Furthermore, CM-Mres eliminated myofibroblasts by inducing an increase in reactive oxygen species (ROS) via NADPH oxidase leading to DNA damage and apoptosis. Moreover, ROS–mediated apoptosis was also induced by CM-Mres in the dormant and outgrowing QDTCs. Overall, our findings suggest for the first time that pro-resolving mediators can target both QDTCs and their permissive niche thus preventing breast cancer from recuring.

Introduction

Breast cancer (BC) that recurs as metastatic disease many years after primary tumor resection and adjuvant therapy appears to arise from tumor cells that disseminated early in the course of the disease [1-4] but did not develop into clinically detectable lesions. These long-term surviving, disseminated tumor cells can maintain a long-lasting state of dormancy (quiescence) (QDTCS) and are resistant to conventional therapies that target actively-dividing cells [1, 5-10] but may be triggered to proliferate through largely unknown mechanisms. Previously we demonstrated that a permissive tumor microenvironment is required for the switch of QDTCs to metastatic outgrowth. In particular, the fibrotic-like niche (FLN) enriched with Type I Collagen (Col-I) was part of the tumor permissive microenvironment. [11-13]. By utilizing a model system based on the D2.0R and counterpart D2A1 mammary cancer cell lines to study dormant vs. metastatic proliferative growth [14-16], we found that metastatic D2A1 cells when cultured in a 3D system (composed of Basement Membrane Extract; BME) transitioned from a dormant to proliferative state upon production of fibronectin, modeling tumor dormancy and outgrowth [11, 17]. Furthermore, metastatic lesions arising from D2A1 cells *in vivo* were associated with significant deposition of fibronectin and Col- I, whereas a related dormant D2.0R cell line did not express fibronectin or Col-I [11-13]. However, supplementing the 3D BME system with fibronectin and/or Col-I induced a transition of D2.0R cells from quiescence to growth. Furthermore, induction of fibrosis, with deposition of Col-I in the metastatic microenvironment *in vivo*, enabled dormant D2.0R cells to form proliferative metastatic lesions [12]. Hence, D2A1 cells were able to escape tumor dormancy by inducing a stromal fibrotic-like response *in vivo*, whereas D2.0R cells required an exogenous fibrotic stimulus to initiate their proliferative response. Importantly, these findings are consistent with several clinical observations demonstrating a correlation between local tissue fibrosis and breast cancer recurrence [13, 18, 19]. Thus, escaping tumor dormancy appears to depend on the generation of a tumor-driven or exogenously-triggered fibrotic-like milieu.

Fibrosis occurs upon dysregulated and exaggerated tissue repair in response to infection or injury, that fails to subside and resolve [20, 21]. It can occur in various organs and involves multiple mediators

that are released into the surrounding milieu. These mediators evoke intracellular signaling pathways in various stromal cells, such as myofibroblasts (which differentiate from fibroblasts), endothelial cells and macrophages, and together with extracellular matrix (ECM) components may be an important triggering event in the metastatic switch of residing QDTC.

Macrophages are a highly diverse immune cell population that, while originating from a common precursor, are also capable of metamorphosing to functionally distinct phenotypes such as M1 (classically-activated) and M2 (alternatively-activated) macrophages. These macrophages play key roles in acute and chronic inflammation, as well as the resolution of inflammation and fibrosis [22-25]. M1 macrophages display a pro-inflammatory phenotype [22, 23]. Conversely, M2-like macrophages promote tissue repair by secreting growth factors such as transforming growth factor beta-1 (TGFβ1) to induce myofibroblast differentiation and deposition of ECM, and angiogenic mediators to promote angiogenesis [25]. Hence, tight temporal regulation of macrophage phenotypes is required to promote resolution of inflammation, tissue repair and reinstatement of homeostasis.

Previously a novel subset of pro-resolving macrophages designated $CD11b^{low}$ macrophages (or Mres) were identified during the resolution phase of acute murine peritonitis [26]. These macrophages secrete pro-resolving mediators and are derived *in vivo* and *ex vivo* from M2-like macrophages following the engulfment of apoptotic leukocytes, which is a hallmark of resolution. However, these macrophages display an enzymatic profile distinct from either M1 or M2, are devoid of phagocytic potential, and are prone to migrate to lymphoid tissues [26]. Furthermore, these Mres can produce anti-angiogenic mediators, thereby, ensuring tissue restoration to its homeostatic state [27].

Building on these previous studies we hypothesized that resolution of inflammation is aberrant at the metastatic niche thus leading to chronic inflammation and the formation of a FLN that supports QDTCs outgrowth. This may be due to the absence or under-representation of the pro-resolving mediators that are required to promote resolution of inflammation. Hence, in this study we tested whether reinstating resolution of inflammation by using soluble mediators produced by Mres will inhibit the establishment of a FLN around residing QDTC and in turn, will prevent QDTCs escape

from the dormant state. We found that secreted mediators generated by Mres promoted resolution of inflammation at the metastatic niche where dormant D2A1 cells resided and prevented their escape from the dormant state. These pro-resolving mediators prevented the formation of the FLN by inhibiting fibroblasts differentiation to myofibroblasts and Col-I expression and by inducing myofibroblast apoptosis via oxidative stress. Intriguingly, apoptosis mediated in part by oxidative stress was also induced in the dormant and outbreaking mammary cancer cells, leading to their demise.

Results

Ex-vivo generation of secreted mediators of pro-resolving CD11b^{low} macrophages

To reinstate resolution of inflammation we developed an *ex vivo* protocol for the enrichment of pro-resolving CD11b^{low} macrophages as described previously with some modifications [27]. Specifically, peritonitis was induced (Fig. 1A) and 66 hours later, when resolution of inflammation was already initiated, peritoneal exudates were collected. The percentage of macrophages was determined in the peritoneal exudates, based on their size, granularity (Fig. 1B, see gated area and red arrow) and a F4/80^{+} Ly6G^{-} phenotype (Fig. 1C). The majority of cells in the exudate were macrophages (Fig.1C) as determined by FACS analysis. Furthermore, while 66% of the macrophages were CD11b^{high}, 34% were CD11b^{low} (Fig. 1D-E) indicating that resolution was already initiated *in vivo*. The recovered macrophages (Mφ) were either untreated or treated with apoptotic Jurkat cells (a common apoptotic leukocyte target for macrophages in experimental procedures [28]) at a ratio of 1: 5 Mφ to apoptotic Jurkat cells (AC) respectively (Fig. 1F). The successful conversion to the CD11b^{low}phenotype was assessed by immunostaining and FACS analysis as illustrated in Fig. 1G-H. This ratio of Mφ to AC yielded an optimal conversion of the macrophages to a CD11b^{low} phenotype (from 25% to 75%) (Fig. 1H) and corresponded to a reduction in the number of non-engulfed AC (10%) (data not shown). Conditioned media was recovered during the conversion of CD11b^{high} macrophages to CD11b^{low} macrophages (CM-Mres) and from control cultures: untreated Mφ (CM- Mφ) and un-engulfed AC

(CM-AC). Notably, high levels of Annexin A1; previously shown to be involved in the resolution of inflammation [29], was detected in CM-Mres as compared to CM- Mφ (Fig. 1I). This was further evidence that the macrophages have acquired a pro-resolving phenotype [30].

Metastatic outgrowth of dormant tumor cells is inhibited by soluble mediators secreted by *ex-vivo* generated pro-resolving macrophages.

Macrophages are highly plastic cells that change their properties upon interaction with tumor cells and their niche [31]. Therefore, we generated culture media from *ex-vivo* generated pro-resolving CD11b^{low} macrophages (CM-Mres), rather than using the cells themselves, and evaluated the metastasis-limiting properties of secreted mediators in it. Since a FLN is required for the switch of QDTC to metastatic outgrowth [11-13], we explored whether promoting the resolution axis locally using CM-Mres may prevent the establishment of the permissive niche and in turn hinder the outbreak of dormant D2A1 cells. To this end lungs of mice (3 mice per group) were either untreated or preconditioned by nasal administration (every 48h) with the relevant conditioned media [culture medium (designated CM), CM-Mφ and CM-Mres]. On day 4, experimental metastases were generated by inoculating all mice with 5x10^5 D2A1 cells stably-expressing GFP (D2A1-GFP cells). The respective conditioned media were continually administered as described above every 48h until day 15 (Fig. 2A). All mice were sacrificed on day 18 and lungs harvested, formalin fixed and paraffin embedded. Histological analysis of paraffin-embedded lung sections revealed that treatment with CM-Mres significantly reduced the incidence of metastatic lesions in the lungs as compared to untreated lungs and lungs treated with either CM or CM-Mφ (Fig. 2B). Furthermore, using single cell organ microscopy (SCOM) to image tumor cells on the entire surface of the lung, we found that CM or CM-Mφ enhanced the metastatic potential of D2A1-GFP cells relative to their metastatic potential in untreated mice (SCOM, Fig. 2C). This may be due to the presence of growth factors (10% FBS and 10% FBS plus CD11b^{high} macrophages-secreted mediators, respectively) in these conditioned media, highlighting the marked effect of preconditioning and treatment of the lungs with CM-Mres

(also containing 10% FBS) that could reduce metastatic outgrowth to levels beneath the untreated controls (Fig. 2C). To test whether CM-Mres can maintain D2A1-GFP cells in a dormant state in the lungs, we repeated the experiment above (4-8 mice per group) using lower numbers of D2A1-GFP cells ($200x10^3$ cells/mouse). Tumor cells on the surface of the lungs were imaged by SCOM (Fig. 2D) [11, 12, 67, 72] . Where fluorescence surface area of >1200 μm^2 represented multi-cellular proliferative metastatic lesions, whereas foci of ≤1200 μm^2 indicated individual dormant metastatic cells (Fig. 2D upper panel). Our results (Fig. 2D lower panel) revealed a significant decrease in the percentage of outbreaking D2A1-GFP lesions between mice treated with CM-Mres (30% outbreaking) vs. CM-Mφ (70% outbreaking). Furthermore, the total tumor burden in lungs treated with CM-Mres was significantly lower (~4-fold reduction) compared to the total tumor burden in lungs treated with CM-Mφ (Fig. 2E). Importantly, no evidence of physical distress upon treatment was apparent in any of the treated mice. Overall, our results demonstrate that soluble factors secreted by Mres can significantly inhibit the outgrowth of dormant D2A1-GFP cells even in the presence of exogenous growth factors.

We next tested whether the CM-Mres promoted resolution of inflammation at the metastatic site. We tested whether CM-Mres induced immune silencing of alveolar macrophages (AM), given previous reports demonstrating that macrophages will undergo immune-silencing thus preventing unwanted excessive inflammatory responses during the resolution phase of inflammation [32]. To this end, bronchoalveolar lavage (BAL) fluids and AM were isolated as described previously [33] from lungs of mice inoculated with D2A1-GFP (one week and two weeks post inoculation) and treated with the different conditioned media. The AM were activated with LPS (1μg/ml) *in vitro* for over-night stimulation and secretion of the pro-inflammatory cytokines IL-12 and TNF-α was analyzed by standard ELISA. We observed a significant reduction in IL-12 and TNF-α levels in the conditioned media of LPS-treated AM derived from CM-Mres treated (AM-Mres) as compared to CM-Mφ-treated (AM- Mφ) mice (Fig. 2F), suggesting that CM-Mres promoted immune silencing of the AM at the metastatic niche.

Notably, within the outbreaking metastatic lesions we observed Col-I fibers (Fig. 2G and Fig. 2H ,indicated by white arrow) as previously described [12], whose spatial distribution was similar to the location of alpha-smooth muscle actin (α-SMA)$^+$ myofibroblasts (Fig. 2H, indicated by black arrows) suggesting that myofibroblasts were the source of Col-I production in the lungs.

CM-Mres prevents metastatic outbreak of dormant tumor cells co-cultured with myofibroblasts *in vitro*.

During normal wound healing and resolution of inflammation, myofibroblasts are transiently present and play an important role in the remodeling of the recuperating tissue. However, when persistent in tissues, they are a well-recognized early histological marker of progressive organ fibrosis, displaying uncontrolled activation. This, in turn results in excessive deposition of ECM components such as Col-I [34]. Hence, we next examined whether CM-Mres prevented the outgrowth of dormant tumor cells in the lungs by inhibiting proliferation and Col-I expression by myofibroblasts. To this end we employed a 3D BME system to model tumor dormancy and outgrowth [17]. In this system, we previously demonstrated that supplementation with Col-I induced the transition of persistently dormant D2.0R cells from quiescence to proliferative growth [12]. We aimed to determine whether mouse embryonic fibroblasts (MEF) (stained only with DAPI, blue) cultured in the 3D BME system (containing TGFβ1) will successfully differentiate to myofibroblasts expressing Col-I (red), and consequently induce dormant D2.0R cells expressing GFP (D2.0R-GFP cells; green) in their vicinity (co-culture) to outbreak (as illustrated in Fig. 3A). Importantly, MEF are widely used as a model to study fibroblasts differentiation to myofibroblasts [35, 36]. In addition, we determined whether exposure to CM-Mres would prevent this outbreak. Our results indicate that MEF cultured in the 3D BME system differentiated to myofibroblasts, as determined by their expression of Col-I (Fig. 3B, D-E and supplementary Fig. 1). Treatment of differentiating MEF with CM-Mres significantly reduced the expression of Col-I and inhibited their proliferation in comparison to treatment with either CM-Mφ or CM-AC (Fig. 3E-F). Furthermore, co-culture of dormant D2.0R-GFP cells with differentiating

MEF in the 3D BME system lead to their outbreak, and this was significantly inhibited by treatment with CM-Mres (Fig. 3B-C and supplementary Fig. 1).

CM-Mres inhibits fibroblasts differentiation to myofibroblasts independent of TGFβ1 canonical signaling.

TGFβ1 is a master regulator of fibroblasts to myofibroblasts differentiation [37] and is present in the 3D BME system. We therefore aimed to determine whether CM-Mres inhibits TGFβ1-induced differentiation of the MEF to myofibroblasts. Differentiated MEF were identified based on increased proliferation, expression of α–SMA, a key marker of myofibroblast differentiation [38, 39], and expression and deposition of Col- I [34]. To this end serum starved MEF were pre-treated with either CM-Mres or with the relevant controls; CM (containing 10% FBS, control), CM-Mφ or CM-AC (prepared as described in Fig. 1). This was followed by TGF-β1 (1ng/ml) exposure for 72h as illustrated in Fig. 4A. We found that CM-Mres significantly inhibited TGF-β1-induced MEF proliferation (Fig. 4B) in comparison to CM-Mφ and this was due to a significant increase in cell cycle arrest at the G0/G1 phase (64% vs. 38% respectively; Fig. 4C-D). In addition, CM-Mres significantly reduced the expression of α-SMA (Fig. 4E) and abolished Col-I expression at both the mRNA and protein levels (Fig. 4F-G) in CM-Mres- treated, as compared to either CM-Mφ or CM-AC-treated MEF. Notably, our results indicate that the inhibition of MEF differentiation by CM-Mres was not due to inhibition of the TGFβ1 canonical signaling pathway, since the phosphorylation of Smad2 and Smad3 was not inhibited (Supplementary Fig.2A-C). Furthermore, non-canonical signaling induced by TGFβ1, such as ERK phosphorylation [37], was not altered significantly upon treatment with CM-Mres (Supplementary Fig.2D-E). Hence, the inhibition of MEF differentiation to myofibroblasts by CM-Mres was not due to inhibition of TGFβ1 canonical signaling.

CM-Mres promotes deactivation of myofibroblasts and apoptosis by inducing oxidative stress. Our previous results indicate that CM-Mres inhibits the differentiation of fibroblasts to myofibroblasts. During the termination of wound repair myofibroblasts cease to proliferate and produce Col-I, and undergo apoptosis to restore tissue architecture [reviewed in [40]]. Therefore, we examined whether CM-Mres will trigger myofibroblast inactivation and apoptosis as illustrated in Fig. 4H. CM-Mres inhibited the proliferation of myofibroblasts derived from isolated mouse lung fibroblasts as compared to untreated or CM-Mφ treated myofibroblasts (Fig. 4I). Similarly, CM-Mres significantly inhibited the proliferation of MEF- derived myofibroblasts by inducing G0/G1 arrest (72% vs. 33% and 29% untreated or CM-Mφ- treated respectively; Fig. 4J-L).

Notably, CM-Mres abolished Col-I expression in MEF-derived myofibroblasts at both the mRNA and protein levels (Fig. 4M-N) and also significantly inhibited fibronectin expression (Fig 4O). Taken together, our results suggest that CM-Mres inhibits Col-I production at the metastatic site by inhibiting fibroblast to myofibroblast differentiation and promoting myofibroblast inactivation. Myofibroblast apoptosis is one of the hallmarks of wound repair resolution, therefore, we next tested whether CM-Mres induced myofibroblast apoptosis. Indeed, CM-Mres promoted apoptosis of myofibroblasts that were differentiated from MEF as indicated by the increase in the percentage of cells that stained positively for Annexin V and PI (late apoptosis) (~ 3-fold increase) compared to untreated or CM-Mφ treated myofibroblasts (Fig. 5A-B). Furthermore, treatment of myofibroblasts with CM-Mres induced the expression of activated caspase 9 after 1h followed by downstream activation of executioner caspases; caspase 7 and caspase 3 after overnight treatment (Fig. 5C). Moreover, Q-VD-OPh, a pan-caspase inhibitor, attenuated significantly the inhibition of myofibroblasts proliferation by CM-Mres (Fig. 5D). Hence, the data demonstrates that CM-Mres induced intrinsic apoptosis of myofibroblasts.

The naturally occurring intrinsic apoptotic pathway is triggered by DNA damage, oxidative stress, or oncogene activation. Therefore, we initially tested whether apoptosis was induced as a result of DNA damage by measuring γH2AX-the phosphorylated form of H2AX that is activated upon formation of

double strands breaks (DSB)[41]. Indeed, γH2AX was detected only in myofibroblasts treated with CM-Mres compared to treatment with either CM or CM-Mφ. (Fig. 5E). Given that DNA damage can result from imbalance in reactive oxygen species (ROS), we next measured ROS levels in CM-Mres-treated myofibroblasts. Notably, ROS are short lived small molecules. We therefore assessed ROS levels at different time points starting at 30 min, post treatment. Our results revealed a significant and transient increase in ROS levels (~1.5-fold increase) at 3h post treatment in CM-Mres–treated as compared to CM-Mφ–treated myofibroblasts (Fig. 5F-G). Furthermore, in the presence of ROS scavenger, N-Acetyl-L-cysteine (NAC, 10 mM), there was a decrease in CM-Mres induced γH2AX (Fig. 5E). Hence an increase in ROS levels upon treatment with CM-Mres induced DNA damage in myofibroblasts.

Ataxia teleangiectasia mutated (ATM) protein was shown previously to be activated by ROS and in response to DSB formation, and is considered a major physiological mediator of H2AX phosphorylation in response to DNA damage [41]. ATM is activated when autophosphorylated at Ser1981 (pATM). Figure 5H-I demonstrates a 3-fold increase in the percentage of myofibroblasts positive for nuclear pATM upon CM-Mres treatment in comparison to treatment with CM-Mφ and a significant reduction in CM-Mres-induced nuclear pATM was apparent in the presence of the ROS scavenger NAC (NAC, 10 mM). Furthermore, NAC significantly attenuated CM-Mres-mediated inhibition of cell proliferation and Caspase3/7 activation in myofibroblasts (Fig. 5J-L). Overall, our data demonstrates that CM-Mres induced a transient oxidative stress in myofibroblasts, culminating in DNA damage and induction of apoptosis.

Next, we explored whether increased ROS levels induced stress signals by phosphorylating JNK (p-JNK) and p38 (p-p38) that in turn, may activate cell cycle arrest or the intrinsic apoptosis pathway[42, 43]. Indeed, CM-Mres treatment for 30 min significantly increased p-p38 and p-JNK levels as compared to either CM-Mφ or CM treatment and NAC significantly inhibited this effect (Fig. 6A and B). However, inhibition of p-38 by SB 203580 (15μM) and JNK activation/phosphorylation by SP600125 (0.2μM) (Fig. 6C) failed to inhibit CM-Mres induced apoptosis (Fig. 6C-E). Higher

concentrations of either SB 203580 (30 μM) or SP600125 (20 μM), reported in the literature to inhibit either JNK or p38 activation respectively (as seen in Fig. 6C), induced apoptosis of CM treated cells and increased CM-Mres apoptotic activity (data not shown). Hence, an increase in ROS levels induced stress signals such as p38 and JNK, but these stress signals did not mediate ROS-induced apoptosis. Interestingly, the JNK inhibitor also inhibited CM-Mres induced p-p38 (Fig. 6C), suggesting that p-JNK mediated p38 phosphorylation. We next tested whether CM-Mres inhibited myofibroblast viability by increasing the levels of the free radical nitric oxide (NO^-) (Fig. 6F), given that NO^- can induce DNA damage and apoptosis [44]. To this end myofibroblasts were treated with CM-Mres in the absence or presence of increasing concentrations of L-NAME, a nitric oxide synthase (NOS) inhibitor, for 24h. Figure. 6G demonstrates a significant increase in activated caspase3/7 in myofibroblasts upon treatment with CM-Mres as compared to CM-Mφ, and this was not altered by the addition of L-NAME (50μM), suggesting that CM-Mres did not induce apoptosis by increasing NO- production within the cells. However, CM-Mres did increase superoxide/O_2^- levels in myofibroblasts as early as 15 min post-myofibroblasts treatments (Fig. 6H). To further validate our findings, we tested caspase3/7 activity in myofibroblasts that were treated with CM-Mres in the presence or absence of the superoxide dismutase (SOD) mimetic MnTBAP (Fig.6F and Fig.6I). Importantly, SOD plays pivotal roles in the protection against ROS-mediated oxidative damage at the initial stage by rapidly catalyzing the conversion of superoxide into oxygen and hydrogen peroxide (H_2O_2) (Fig. 6F). Indeed, MnTBAP (100μM) significantly decreased the CM-Mres-induced caspase3/7 activity (Fig. 6I), providing additional evidence that CM-Mres induced apoptosis by increasing the levels of superoxide. Superoxide is produced by several endogenous sources such as mitochondrial electron transport chain and NADPH oxidases (NOX) [45](Fig. 6F). We demonstrate that in the presence of Diphenyleneiodonium chloride (DPI), a pan inhibitor of NOX, there was a significant decrease in CM-Mres-induced caspase3/7 activity (Fig. 6J). Taken together, our data suggest that CM-Mres induced a transient increase in superoxide levels in myofibroblasts via NOX activation resulting in DNA damage and apoptosis.

CM-Mres promotes apoptosis of dormant and outbreaking breast tumor cells by inducing oxidative stress *in vitro.*

Our finding that CM-Mres can induce oxidative stress in myofibroblasts leading to their apoptosis *in vitro* raised the possibility that CM-Mres also prevented the outgrowth of dormant D2A1 cell at the metastatic site by the same mechanism. To address this question, we used D2.0R cells that are dormant in lungs of mice and in our 3D BME system and D2A1 cells which display a transient dormant phase both *in vitro* and *in vivo* [11, 12, 16]. Both cell lines were cultured in the 3D BME system and treated in their dormant phase (day 3 for D2A1 and for D2.0R cells) (Fig. 7A) or during outbreak (day 1 of D2.0R cells when cultured in 3D BME system supplemented with Col-I) (Fig. 7B) with the different conditioned media for 1 hour to determine ROS levels. We found a significant increase in ROS levels (~1.2-fold increase) in CM-Mres-treated as compared to CM-Mφ –treated cells. Moreover, as shown in Fig. 7C, CM-Mres induced cell death in dormant D2.0R and D2A1 cells and in outbreaking D2.0R cells, as evidenced by a dramatic decline in cell number per field compared to control and the presence of punctuated cells. In addition, the dying cells were positively stained for TUNEL assay (Fig. 7D), suggesting that apoptosis was induced. Quantifying cell viability by Calcein AM staining demonstrated a significant decrease in cell viability in both dormant and outbreaking cells in the 3D BME system after 72h treatment with CM-Mres (Fig. 7E). Finally, CM-Mres induced apoptosis of both dormant and outbreaking cells as demonstrated by a significant increase in caspase3/7 activity (~3-fold increase) after a 24h treatment and this was significantly inhibited by the addition of NAC (Fig. 7F).

Taken together, our results indicate that CM-Mres promotes apoptosis in dormant and outbreaking mammary cancer cells by increasing their oxidative stress.

Discussion

The major threat to breast cancer patients' survival is recurrence, as metastatic disease, which can occur after long latency periods. Most therapies that target dividing cancer cells fail in the dormant

metastatic setting since these DTCs are non-dividing. Thus, it is vital to develop new therapeutic strategies to confront dormant DTCs before their emergence to overt metastases. One such novel strategy that has evolved over the years to confront metastatic disease is immunotherapy. For example, targeting the survival of tumor associated macrophages (TAM) that display an M2-like phenotype or promoting their repolarization to tumor-suppressive M1-like TAMs has been proposed (reviewed in [46]). Although immunotherapies of various types have been successfully used for the treatment of some cancers [47], they were not found to be effective against breast cancer metastases. Here, we introduce a novel approach to abrogating metastatic breast cancer that consists of limiting and terminating the tissue repair process manipulated and exaggerated by outbreaking metastases. This approach restores a homeostatic state rather than attempts to provoke immune responses that allow inflammation to persist. In this study, we demonstrate for the first time that converting the FLN to a homeostatic state by promoting the resolution process resulted in two beneficial outcomes 1) it prevented the establishment of a permissive microenvironment for disease recurrence and this was driven by bioactive mediators secreted by *ex-vivo* enriched pro-resolving CD11b^{low} macrophages (CM-Mres) and 2) it significantly hindered the outgrowth of dormant mammary DTCs by inducing their apoptosis.

These findings are in line with a recent report demonstrating how preoperative stimulation of resolution of inflammation by introducing resolvins along with inflammation blockage prevented micrometastases and recurrence in Lewis lung carcinoma [48].

The important role of the FLN in modulating the colonization of DTCs [49-53] as well as their emergence from dormancy to metastatic growth [11-13] was demonstrated by several research groups. Furthermore, several studies attempted to target the FLN in order to improve therapy response [19, 54, 55]. Our results demonstrate that modulating the FLN in the 3D BME co-culture system by inhibiting Col-I expression can maintain DTCs in a dormant state. Moreover, treating the lungs with soluble mediators secreted by pro-resolving CD11b^{low} macrophages maintained 70% of the metastatic lesions of D2A1-GFP cells dormant as compared to only 30% in lungs treated with CM-Mφ and reduced by 4-fold the

339 total metastatic burden per lung. Hence, our results demonstrate that CM-Mres can significantly
340 inhibit the outgrowth of dormant D2A1-GFP cells in the presence of exogenous growth factors.
341 Notably, successful resolution of inflammation is marked by immune-silencing of macrophages to
342 prevent unwanted excessive inflammatory responses during the resolution phase of inflammation.
343 We documented immune-silencing of alveolar macrophages (AM) that were derived from lungs
344 inoculated with D2A1-GFP cells and treated with CM-Mres. Specifically, a significant reduction in
345 pro-inflammatory cytokines IL-12 and TNF-α levels in the conditioned media of LPS-treated AM
346 derived from lungs of CM-Mres–treated mice compared to controls was observed. This suggests that
347 resolution of inflammation has occurred at the metastatic site

348 Upon hampered resolution of inflammation, myofibroblasts in the lung produce a fibrotic niche [56]
349 and persist. Our results indicate that CM-Mres inhibits Col-I expression in myofibroblasts and
350 thereby limits ECM deposition and hinders the outgrowth of dormant tumor cells. Our 3D BME
351 system showed that co-culture of MEF with otherwise dormant D2.0R cells induced the outgrowth
352 of the latter. Treatment with CM-Mφ enhanced Col-I deposition by the differentiating MEF,
353 confirming that $CD11b^{high}$ macrophages possess an M2-like phenotype [26, 27, 32]. Treatment with CM-
354 Mres, on the other hand, limited myofibroblast expansion, abolished their Col-I expression and
355 deposition (thereby underpinning the pro-resolving nature of $CD11b^{low}$ macrophages) and kept
356 D2.0R cells dormant. These findings are in agreement with our previous work demonstrating the role
357 of Col-I in instigating the outgrowth of dormant D2.0R cells [11, 12].

358 Notably, successful resolution of inflammation depends on inhibition of fibroblast differentiation to
359 myofibroblasts and apoptosis of active myofibroblasts [reviewed in [40]]. Along these lines, we found
360 that CM-Mres inhibited TGFβ1-induced differentiation of MEF to myofibroblasts as evidenced by a
361 decrease in MEFs proliferation. The majority of MEF (64%) were growth arrested at the G0/G1
362 phase. Furthermore, CM-Mres abolished Col-I expression at both the mRNA and protein levels and
363 significantly decreased α-SMA expression. Surprisingly, this inhibition was independent of TGFβ1

canonical signaling. We also found that CM-Mres impacts myofibroblasts by promoting their cell cycle arrest, apoptosis, and inhibits Col-I and fibronectin expression. Hence CM-Mres, in addition to inhibiting fibroblast differentiation and activation, can also deactivate myofibrobalsts. Notably, these functions are all characteristic of the normal physiology of tissue repair during the resolution process [56]. Intriguingly, a previous report by Popov and colleagues demonstrated that macrophage-mediated phagocytosis of apoptotic cholangiocytes contributed to the reversal of experimental biliary fibrosis [57]. These findings highlight the link between the engulfment of apoptotic cells by macrophages as part of the resolution of inflammation and their anti-fibrotic properties.

Importantly, we found that CM-Mres induced a transient increase in ROS levels in myofibroblasts followed by induction of stress signals (p38 and JNK), DNA damage, cell cycle arrest and apoptosis. Whereas, ROS scavenger (NAC) significantly attenuated CM-Mres-induced p38 and JNK phosphorylation/activation, γH2AX expression (a sensor of DNA damage) and phosphorylation of ATM. In addition, NAC significantly inhibited CM-Mres induced caspase3/7 activity. Overall, this confirms that CM-Mres induced apoptosis of myofibroblasts by promoting oxidative stress. Interestingly, pharmacological inhibition of CM-Mres-induced p38 or JNK activation did not inhibit CM-Mres induced-apoptosis. Overall, the data suggest that activation of p38 and JNK by CM-Mres was part of a myofibroblasts defense mechanism , culminating in their cell cycle arrest in response to cellular stress [58, 59].

ROS are small, highly reactive and short-lived molecules. They can be oxygen-derived free radicals like superoxide anion ($O_2^{\bullet-}$) and the hydroxyl radical ($OH^{\bullet}$), or non-radical molecules such as hydrogen peroxide (H_2O_2). The generation of ROS in cells exists in equilibrium with a wide variety of antioxidant defenses including enzymatic and non-enzymatic scavengers such as SOD, and glutathione (GSH), respectively. However, if the antioxidant detoxification systems fail to maintain low, tolerated levels of ROS, then excess cellular levels of ROS can be deleterious and trigger oxidative stress [60]. Notably, TGF-β1 was previously shown to increase ROS production and decrease the concentration of GSH in differentiating fibroblasts [61]. Furthermore, low or moderate levels of

ROS were previously reported to mediate fibroblasts differentiation to myofibroblasts. Specifically, H_2O_2 generation by NADPH oxidase 4 (NOX4) was show to be required for TGF-β1-mediated fibrogenesis in a murine model of lung fibrosis, and similar data were obtained for human fibroblasts *in vitro* [62, 63]. Collectively, these previous findings suggest a higher oxidative stress in myofibroblasts at their basal state. Previous studies have also demonstrated an increased susceptibility of myofibroblasts to apoptotic signals during the resolution phase of wound healing [64]. Therefore, based on these previous observations, one can postulate that an additional increase in ROS levels in myofibroblasts will cause deleterious effects that may result in apoptosis. Various lines of evidence have indicated a critical role for ROS during the natural resolution of inflammation and tissue regeneration/repair by promoting apoptosis of cells such as neutrophil and endothelial cells [65]. Intriguingly, we find that CM-Mres induced a transient and moderate increase in ROS levels that was sufficient to induce myofibroblast apoptosis while ROS scavenging with NAC or adding SOD mimetics or a NOX pan inhibitor significantly inhibited the apoptosis induced by CM-Mres. Hence, the results suggest that CM-Mres triggered the apoptotic cascade as part of resolution of inflammation by promoting a transient increase in $O2^{-}$ levels produced by NOX in myofibroblasts (Fig. 6H and Fig. 8). Indeed, $O2^{-}$ is considered the primary ROS and is easily converted to other ROS, thus triggering a chain of reactions that can lead to apoptosis [45].

In addition to the anti-fibrotic activity of the pro-resolving mediators, we demonstrate for the first time that these physiological mediators secreted by pro-resolving macrophages can promote apoptosis of dormant mammary tumor cells and mammary tumor cells escaping their dormant state by increasing their ROS levels. Whereas, in the presence of NAC there was a significant decrease in activated caspase3/7. Increase in ROS has been reported to play a role during tumorigenesis and spread of the tumor cells to distant organs [66]. Here we demonstrate that dormant DTCs are susceptible to the rise of ROS levels that can lead to their demise by promoting apoptosis. These finding are in line with a previous study by Laura Vera-Ramirez *et al* [67] demonstrating that inhibition of the autophagic flux in D2.0R cells lead to the accumulation of damaged mitochondria and ROS, resulting

in cell apoptosis. Whether CM-Mres induced an increase in ROS levels by inhibiting the autophagic flux in dormant D2.0R and D2A1 cells warrants future studies. Intriguingly, a recent report by Sarah B. Crist and colleagues demonstrated that single dormant breast DTCs found in skeletal muscle and lung exhibit increased oxidative stress. However, DTCs in skeletal muscle rarely emerge from their dormant state given that in the skeletal muscle DTCs are exposed to sustained oxidative stress which results in the induction of endogenous ROS and a highly-oxidized state. Conversely, breast DTC emerge from their dormant state in the lung by reducing oxidative stress [68]. Similarly, oxidative stress was shown previously to limit distant metastasis by melanoma cells *in vivo* [69]. Building on these finding it is conceivable that DTCs must overcome oxidative stress in order to successfully colonize and survive at distant organs and finally emerge from their dormant state. Furthermore, our findings suggest that one may exploit DTCs high oxidative state in order to compromise dormant DTCs survival, by further increasing their ROS levels. Notably, chemotherapies such as doxorubicin (DOX) cause oxidative stress in proliferating tumor cells. However dormant DTCs are resistant to DOX treatment [7]. Therefore, future investigations regarding the identity of the pro-resolving mediator/s that successfully promoted oxidative stress and apoptosis in dormant/quiescent DTCs is warranted. Taken together, our findings provide a proof of concept by which natural products of the normal healing process secreted by pro-resolving macrophages can inhibit the formation of the permissive 'soil' required for the outgrowth of QDTC, thus preventing their metastatic outgrowth. Hence, future identification of these pro-resolving mediators may serve as a basis for the development of novel therapeutic strategies for prevention and treatment of breast cancer recurrence and fibrotic diseases.

Methods

Cell line cultures

D2.0R and D2A1 mouse mammary cancer cells (kindly provided by Prof. Ann Chambers, London Cancer Center, Ontario [16]) and Mouse Embryonic Fibroblast (MEF) (kindly provided by Prof. Sarit Larisch, University of Haifa, Haifa, Israel [70]) were grown in Dulbecco's modified Eagle's medium

(DMEM; Gibco life technology) supplemented with 10% fetal bovine serum (FBS) and antibiotics (Biological Industries, Israel). Jurkat T cells (obtained from Prof. Debbie Yablonski, Technion, Israel) were maintained in RPMI-1640 (Gibco-life technology) with 10% heat inactivated FBS, and antibiotics. D2A1-GFP and D2.0R-GFP cells were prepared by lentiviral infection of D2.0R and D2A1 cells using the FUGW (Addgene plasmid #14883) lentiviral expression vector. Sorting of D2.0R-GFP/D2A1-GFP cells was performed using Sony MA900. All cells were incubated at 37°C, 5% CO2 incubator.

Isolation of mouse lung fibroblasts

Lobes of lungs excised from female BALB/c mice were diced and the fragments were cultured on a slotted 24 well plate and overlaid with DMEM supplemented with 20% fetal bovine serum, antibiotics and 10 ng/ml TGFβ1 [71]. Upon reaching 50 % confluency, the cells were harvested from the plates using trypsin-EDTA (Biological Industries) and cultured for further analysis.

Fibroblasts differentiation to myofibroblasts

MEF or lung fibroblasts were serum starved O.N and then treated with TGFβ1 (1ng/ml; PeproTech, Israel) for 24-72 hours.

Proliferation assay

Cells were cultured in 96 wells plate (1.5-2.0 x103 cells/well). At indicated time points the CellTiter 96 AqueousOne Solution cell proliferation assay kit (Promega) was added to the wells for 2 hours to measure cell proliferation according to the manufacturer's instructions. The absorbance was recorded at 490nm.

Western blot analysis

MEF were lysed using whole-cell extract [WCE; 25mM HEPES buffer, pH 7.7, 0.3M NaCl, 1.5mM $MgCl_2$, 0.2mM EDTA, 0.1% Triton X-100, 100µg/ml PMSF and protease inhibitor cocktail (Roche, 1:25 dilution)]. The protein extracts were run by SDS-PAGE (8-10%) followed by transfer to a nitrocellulose membrane. The membrane was blocked for 1h at room temperature (R.T.) either with 5% (w/v) non-fat dried skimmed milk powder in PBS supplemented with 0.05% Tween20 (PBS-T)

or with 3% BSA in TBS-T for detection of phosphorylated proteins. Membranes were then probed either with rabbit anti Annexin A1 (Cat#PA5-27315; Invitrogen, Thermo-Fischer scientific), rabbit anti fibronectin (Cat# ab2413, Abcam) mouse anti-α-SMA (Cat#ab7817; Abcam), rabbit anti-Col-I (Cat#ab34710; Abcam), rabbit anti-p38 (Cat#9212; Cell Signaling), rabbit anti-phospho-p38 (T180/Y182)(Cat#9211S;Cell Signaling), rabbit anti p-SAPK/JNK(T183/Y185) **(**Cat# 9251S, Cell signaling), mouse anti JNK(Cat# SC-7345; Santa-Cruz SC-7345), mouse anti γ-H2AX (Cat# ab26350; Abcam), rabbit anti-cleaved caspase 3 (Cat # 9664; Cell Signaling) or with rabbit anti-mouse GAPDH (Cat#sc25778; SantaCruz biotechnology) at 4°C overnight. Next, the membranes were washed 15 min x3 with either PBS-T or TBS-T for phospho-experiments respectively and incubated with the appropriate HRP-conjugated secondary antibodies (Jackson ImmunoResearch Laboratories, Inc) for 1 hour at R.T. Next, membranes were washed 15 min x3 with PBS-T/TBS-T. Then, WesternBright ECL (Advansta) was added to the membrane for 1min and analyzed using ImageQuant LAS-4000 analyzer (GE Healthcare Life Sciences) & "ImageQuant LAS-4000" software (GE HealthcareLife Sciences). Densitometric analysis was performed using ImageQuant total lab 7 (GE Healthcare Life Sciences).

Cell cycle analysis

MEFs or differentiated myofibroblasts were incubated with 10 μM bromodeoxyuridine (BrdU) for 45 min. Then, the cells were detached with trypsin-EDTA (Biological Industries), washed in PBS and incubated with 50 μl anti-BrdU-APC for 20 min and with 10μl 7-amino-actinomycin D (7-AAD) according to the manufacturer's instructions (BrdU Flow Kit #552598; BD Pharmingen). Flow cytometry was performed using FACSCanto II (BD) and data was analyzed using the FlowJo software (Treestar).

Detection of apoptosis

Apoptosis of myofibroblasts was determined by staining with FITC-conjugated annexin V using a MEBCYTO Apoptosis Kit (MBL # 4700, Nagoya, Japan) according to the manufacturer's recommendations. Flow cytometry was performed as above.

Quantitative real time PCR

RNA was reversed-transcribed using the High Capacity RNA-to-cDNA Kit (Applied Biosystems). The generated cDNA was used as a template for quantitative PCR using the Fast SYBR Green Master Mix kit (Applied Biosystems). Analysis of gene expression was performed with the StepOneTM and StepOnePlusTM Real-Time PCR detection system (Applied Biosystems) using the relative standard curve method. The following PCR primers (forward and reverse, respectively) for mouse GAPDH and Col-I were designed using the Integrated DNA Technologies Inc software. Mouse GAPDH: 5′-ATGGGACGATGCTGGTACTGA -3′ and 5′ TGCTGACAACCTTGAGTGAAAT -3′; Col-I: 5′-GCTCCTCTTAGGGGCCACT -3′ and 5′-CCACGTCTCACCATTGGGG -3′.

Co-culture in the 3D BME system

D2.0R-GFP cells and MEF were harvested from their growth plates using 0.25% trypsin-EDTA. Collected cells were cultured in Cultrex® growth factor reduced Basement Membrane Extract (BME: Trevigen, Inc) as follows: An 8 well chamber glass slide system (Lab-TEK® II, Naperville, IL) was coated with 70µl Cultrex® (protein concentration between 15mg/ml; thickness~1-2mm). D2.0R-GFP cells ($5x10^3$ cells/well) and MEF cells ($6x10^4$) were re-suspended in DMEM with low glucose supplemented with 2% FBS and 2% Cultrex®. Each cell type was either cultured separately or co-cultured with the other on the coated slides. Slides were incubated at 37°C, 5% CO_2.

Immunofluorescence

Staining for Col-I: MEF ($6x10^4$) cultured in 8 well chamber glass slides in 3-dimensional culture, were treated for 5 minutes with cold methanol: acetone mixture containing 0.1% Triton X-100, and fixed for an additional 10 minutes with cold methanol: acetone mixture.

Staining for p-ATM: MEF ($5.0 x10^3$ cells/well) were cultured in 8 well chamber glass slides in 2 dimensional cultures. Cells were treated for 5 minutes with 4% paraformaldehyde (PFA) containing 5% sucrose and 0.1% triton X-100, and fixed for an additional 25 minutes with PFA containing 5% sucrose.

After fixation, the above cells were washed for 10 minutes with PBS and additional 15 minutes with PBS containing 0.05% tween 20 (Sigma). Next the cells were blocked with IF buffer (130 mM NaCl, 7mM Na2HPO4, 3.5mM NaH2PO4, 7.7mM NaN3, 0.1% BSA, 0.2% Triton X-100, 0.05% Tween 20) containing 10% Donkey serum for 1 hour and incubated overnight at 4°C with either goat anti-type I collagen (1:100) (Cat#1310-01; SouthernBiotech) or mouse anti p-ATM (1:250) (Cat# MA1-2020, Invitrogen) together with Alexa Fluor® 488 phalloidin (1:40; Molecular Probes). The cells were washed three times with PBS for 15 minutes each, and incubated for 1 hour with donkey anti-goat or mouse antibody (respectively) conjugated to Alexa Fluor® 649, (Invitrogen) at R.T. Next, the cells were washed as mentioned above and mounted with VECTASHIELD mounting medium with DAPI. The slides were imaged using a Nikon A1-R confocal laser scanning microscope.

Caspase -Glo 3/7 Assay in 2D and 3D culture

MEF cells were seeded in optical white clear bottom 96 well plates ($2x10^3$cells/well). Four hours post seeding the cells were serum-starved overnight in RPMI medium. Differentiation to myofibroblasts was performed using TGFβ1 (1ng/ml) in macrophages growth medium (CM) over night. The cells were pre-treated for 2h prior to treatment with the different conditioned media, either with NAC (Sigma Cat#A9165, 10mM), DPI (Sigma Cat# D2926, 0.1µM), L-NAME (Sigma Cat# N5751,50 µM) or MnTBAP (abcam Cat# ab141496, 100µM). Next the different conditioned media were diluted 1:1 using fresh CM, and were supplemented with the appropriate inhibitor.

3D Culture: D2.0R/D2A1 cells ($3.0 x10^3$ cells/well) were cultured in optical white clear bottom 96 well plates coated with 50 µl Cultrex ® growth factor-reduced basement membrane extract (BME) and /or BME supplemented with Rat tail Type I collagen (Southern biotech, USA) (as described in [12]). Seventy-two hours' post seeding of D2A1/D2.0R cells, NAC designated wells were pre-incubated with 10mM NAC for 2hr, followed by stimulation with different conditioned media for additional 24h. Next, Caspase-Glo® reagent (Promega, USA) was added to the above experiments according to the manufacturer's instructions and plates were kept in dark and incubated at R.T. for 2hr. Luminescence was measured using a plate-reading infinite M200PRO, TECAN luminometer.

CA-AM staining in the 3D cultures

Dormant D2.0R and D2A1 cells: D2A1 and D2.0R cells were seeded in optical-white, 96 well plates coated with 50 µl BME ($3x10^3$ cells/well). Seventy-two hours post seeding (when dormant) the cells were treated with the different conditioned media for additional 72 h.

Outbreaking D2.0R cells: D2.0R cells were seeded in BME supplemented with Rat–tail Col-I (as described in [12]), in optical-white, 96 well plates ($3x10^3$ cells/well). Next different conditioned media were added 4h post seeding for 72h. Cells viability for both experiments was determined using Fluorometric Calcein AM Assay Kit (Cat# ab228556; abcam) according to the manufacturer instructions.

DCFDA /H2DCFDA-Cellular ROS Assay

Myofibroblasts: MEF were cultured in 6 well plates (35.0 $x10^4$ cells/well) and differentiated into myofibroblasts, as described above. After 24hr, NAC designated wells were pre-incubated with 10mM NAC for 2hr, cells were then exposed to stimulation for 0.5h, 2h,3h or 5 hours with the indicated conditioned media. Cells were then washed with 500µl washing buffer x1 [Cellular ROS assay kit (Cat# ab113851, Abcam)] and incubated with 500µl DCFDA (20Mm) for 30 min at 37°C. Samples were analyzed by flow cytometry according to manufacturer protocol.

Dormant D2A1 and D2.0R cells: D2A1 and D2.0R cells (3000 cells/well) were cultured in 96 black-transparent well plate coated with 50ul BME. After 72h the cells were treated for 1hour with the different conditioned media.

Outbreaking D2.0R cells: D2.0R cells (3000 cells/well) were cultured in 96 black-transparent well plate coated with 50ul BME supplemented with Rat tail Col-I. After 72h the cells were treated for 1hour with the different conditioned media.

Cellular ROS levels for both experiments above were determined in plate reader using Cellular ROS assay kit (Cat# ab113851, Abcam) according to manufacturer instructions.

Animals

7-8 weeks old Male C57BL/6, 5-6 weeks female BALB/c- and 8 weeks female BALB/c-nu/nu athymic mice were purchased from Harlan Biotech Israel. All mice were maintained under specific pathogen-free conditions. Care and handling of animals was in compliance with University of Haifa's experimental protocols.

***Ex-vivo* generation of pro-resolving CD11b^{low} macrophages**

Male C57BL/6 mice were injected I.P. with zymosan A (1 mg). After 66 hrs, peritoneal exudates were collected and exudate cells were stained with PE-conjugated rat anti-F4/80. Macrophages were isolated using EasySep PE selection magnetic beads following the manufacturer's instructions (StemCell Technologies). Isolated macrophages were co-stained with FITC-conjugated rat anti-Ly-6G and PerCP-conjugated rat anti-mouse CD11b (Biolegend) and analyzed by FACSCanto II (BD Biosciences) and the FACSDiva software. Jurkat cells were treated with 1 μM staurosporine (Sigma) to induce apoptosis, and washed. Then, peritoneal macrophages were incubated in the presence or absence of apoptotic Jurkat cells (1:5 macrophage to apoptotic cell ratio). After 24h of incubation the cells were washed with phosphate buffered saline (PBS) and overlaid with fresh media for additional 24 hours of incubation. Next, conditioned media was collected and filtered and the macrophages were further characterized for their conversion to the CD11b^{low} phenotype using flow cytometry**.**

Experimental metastasis assays

6-8-week-old female BALB/c-nu/nu athymic mice (3-8 mice per group) were either untreated or preconditioned by intranasal administration (each nasal received 25ul with a P200 pipette every 48h) with the different conditioned media [Culture medium (designated CM), CM- Mφ and CM-Mres) for 4 days. On day 5 experimental metastasis assay was carried out by tail vein injection of D2A1-GFP cells (0.2/0.5x10^6 cells /mouse) labeled with cell tracker CSFE (Sigma) according to the manufacture protocol. The respective conditioned media were continually administered as described above every 48h. 14 days' post D2A1-GFP cell injection the lungs were harvested, inflated with PBS and subjected to fluorescent single cell whole organ microscopy (SCOM)

imaging by fluorescent video-microscopy (Nikon A1R Microscopy) as previously described [11, 12, 67, 72] . 10 X images of the entire external surface of each lung were sequentially captured and analyzed using NIS-Elements AR software to measure the surface area of the metastases. Surface area >1200μm^2 represented multi-cellular, proliferative metastatic lesions, whereas 60 μm^2 >foci ≤1200 μm^2 indicated individual, dormant tumor cells. Total tumor burden/lung was represented by the total sum of the surface area of the metastases on the entire surface of each lung. All mice were maintained under specific pathogen-free conditions.

Immunohistochemical staining

Paraffin blocks were sectioned at 8 μm thick slices. Endogenous peroxidase activity was blocked using 0.3% H_2O_2 in PBS. Antigen retrieval was carried out for α-SMA staining using citrate buffer. Sections were washed and blocked with goat serum (Vector labs USA, cat # S-100) for 1 h and incubated with Mouse anti-αSMA (1:000; Biocare CM033) for 1 hour at R.T. Immunohistochemical detection was performed using ZytoChem Plus (HRP) Polymer anti mouse (cat #ZUC050), developed with DAB for 10 min and counterstained with hematoxylin for 5 min. The Modified Masson's Trichrom staining was carried out with Trichrome Stain Kit (Modified Masson's, MTC; ScyTek laboratories, Life Sciences) according to the manufacturer protocol. Two sequential paraffin sections (5μm) were stained for either collagen bundles with Picro Sirius Red (PSR) staining (as described in [73]) or immunostained for GFP expressing cells using primary antibody for GFP (1:500; Cat # 5450 Abcam) for O.N incubation at 4°C followed by anti-goat Alexa-488 and counterstained with DAPI. PSR was imaged by Nikon A1R confocal microscope. Samples were excited using a 561-nm laser and emission was detected between 635 and 685 nm.

Statistical analysis

Student's unpaired t test was used accordingly. Two tailed p values of 0.05 or less were considered statistically significant. One-way ANOVA test followed by Tukey's multiple comparison test was used accordingly. P-values of 0.05 or less were considered statistically significant.

References

1. Schmidt-Kittler, O. *et al.* From latent disseminated cells to overt metastasis: genetic analysis of systemic breast cancer progression. *Proc Natl Acad Sci U S A* **100**, 7737-7742 (2003).
2. Husemann, Y. *et al.* Systemic spread is an early step in breast cancer. *Cancer Cell* **13**, 58-68 (2008).
3. Hosseini, H. *et al.* Early dissemination seeds metastasis in breast cancer. *Nature* (2016).
4. Harper, K.L. *et al.* Mechanism of early dissemination and metastasis in Her2(+) mammary cancer. *Nature* (2016).
5. Pantel, K. *et al.* Differential expression of proliferation-associated molecules in individual micrometastatic carcinoma cells. *J Natl Cancer Inst* **85**, 1419-1424 (1993).
6. Aguirre-Ghiso, J.A. Models, mechanisms and clinical evidence for cancer dormancy. *Nat Rev Cancer* **7**, 834-846 (2007).
7. Naumov, G.N. *et al.* Ineffectiveness of doxorubicin treatment on solitary dormant mammary carcinoma cells or late-developing metastases. *Breast Cancer Res Treat* **82**, 199-206 (2003).
8. Sosa, M.S., Bragado, P. & Aguirre-Ghiso, J.A. Mechanisms of disseminated cancer cell dormancy: an awakening field. *Nat Rev Cancer* **14**, 611-622 (2014).
9. Pantel, K. & Woelfle, U. Micrometastasis in breast cancer and other solid tumors. *J Biol Regul Homeost Agents* **18**, 120-125 (2004).
10. Sauer, S. *et al.* Innovative Approaches in the Battle Against Cancer Recurrence: Novel Strategies to Combat Dormant Disseminated Tumor Cells. *Front Oncol* **11**, 659963 (2021).
11. Barkan, D. *et al.* Inhibition of metastatic outgrowth from single dormant tumor cells by targeting the cytoskeleton. *Cancer Res* **68**, 6241-6250 (2008).
12. Barkan, D. *et al.* Metastatic growth from dormant cells induced by a col-I-enriched fibrotic environment. *Cancer Res* **70**, 5706-5716 (2010).
13. Barkan, D., Green, J.E. & Chambers, A.F. Extracellular matrix: A gatekeeper in the transition from dormancy to metastatic growth. *Eur J Cancer* **46**, 1181-1188 (2010).
14. Morris, V.L. *et al.* Mammary carcinoma cell lines of high and low metastatic potential differ not in extravasation but in subsequent migration and growth. *Clin Exp Metastasis* **12**, 357-367 (1994).
15. Morris, V.L., Tuck, A.B., Wilson, S.M., Percy, D. & Chambers, A.F. Tumor progression and metastasis in murine D2 hyperplastic alveolar nodule mammary tumor cell lines. *Clin Exp Metastasis* **11**, 103-112 (1993).
16. Naumov, G.N. *et al.* Persistence of solitary mammary carcinoma cells in a secondary site: a possible contributor to dormancy. *Cancer Res* **62**, 2162-2168 (2002).
17. Barkan, D. & Green, J.E. An In Vitro System to Study Tumor Dormancy and the Switch to Metastatic Growth. *J Vis Exp* **11**, 54 (2011).
18. Hasebe, T. *et al.* Prognostic significance of fibrotic focus in invasive ductal carcinoma of the breast: a prospective observational study. *Mod Pathol* **15**, 502-516 (2002).
19. Rybinski, B., Franco-Barraza, J. & Cukierman, E. The wound healing, chronic fibrosis, and cancer progression triad. *Physiol Genomics* **46**, 223-244 (2014).
20. Stramer, B.M., Mori, R. & Martin, P. The inflammation-fibrosis link? A Jekyll and Hyde role for blood cells during wound repair. *J Invest Dermatol* **127**, 1009-1017 (2007).
21. Nathan, C. & Ding, A. Nonresolving inflammation. *Cell* **140**, 871-882 (2010).
22. Mantovani, A. *et al.* The chemokine system in diverse forms of macrophage activation and polarization. *Trends Immunol* **25**, 677-686 (2004).
23. Martinez, F.O., Helming, L. & Gordon, S. Alternative activation of macrophages: an immunologic functional perspective. *Annu Rev Immunol* **27**, 451-483 (2009).
24. Weigert, A., Jennewein, C. & Brune, B. The liaison between apoptotic cells and macrophages--the end programs the beginning. *Biol Chem* **390**, 379-390 (2009).

25. Wynn, T.A. & Vannella, K.M. Macrophages in Tissue Repair, Regeneration, and Fibrosis. *Immunity* **44**, 450-462 (2016).
26. Schif-Zuck, S. *et al.* Saturated-efferocytosis generates pro-resolving CD11b low macrophages: modulation by resolvins and glucocorticoids. *Eur J Immunol* **41**, 366-379 (2011).
27. Michaeli, S. *et al.* Soluble Mediators Produced by Pro-Resolving Macrophages Inhibit Angiogenesis. *Front Immunol* **9**, 768 (2018).
28. Lawrence, T. Inflammation and cancer: a failure of resolution? *Trends Pharmacol Sci* **28**, 162-165 (2007).
29. Sugimoto, M.A., Sousa, L.P., Pinho, V., Perretti, M. & Teixeira, M.M. Resolution of Inflammation: What Controls Its Onset? *Front Immunol* **7**, 160 (2016).
30. Purvis, G.S.D., Solito, E. & Thiemermann, C. Annexin-A1: Therapeutic Potential in Microvascular Disease. *Front Immunol* **10**, 938 (2019).
31. Dehne, N., Mora, J., Namgaladze, D., Weigert, A. & Brune, B. Cancer cell and macrophage cross-talk in the tumor microenvironment. *Curr Opin Pharmacol* **35**, 12-19 (2017).
32. Ariel, A. & Serhan, C.N. New Lives Given by Cell Death: Macrophage Differentiation Following Their Encounter with Apoptotic Leukocytes during the Resolution of Inflammation. *Front Immunol* **3**, 4 (2012).
33. Busch, C.J., Favret, J., Geirsdottir, L., Molawi, K. & Sieweke, M.H. Isolation and Long-term Cultivation of Mouse Alveolar Macrophages. *Bio Protoc* **9** (2019).
34. Klingberg, F., Hinz, B. & White, E.S. The myofibroblast matrix: implications for tissue repair and fibrosis. *J Pathol* **229**, 298-309 (2013).
35. Sousa, A.M. *et al.* Smooth muscle alpha-actin expression and myofibroblast differentiation by TGFbeta are dependent upon MK2. *J Cell Biochem* **100**, 1581-1592 (2007).
36. Vaahtomeri, K. *et al.* Lkb1 is required for TGFbeta-mediated myofibroblast differentiation. *J Cell Sci* **121**, 3531-3540 (2008).
37. Biernacka, A., Dobaczewski, M. & Frangogiannis, N.G. TGF-beta signaling in fibrosis. *Growth Factors* **29**, 196-202 (2011).
38. Phan, S.H. Genesis of the myofibroblast in lung injury and fibrosis. *Proc Am Thorac Soc* **9**, 148-152 (2012).
39. Shukla, A. *et al.* CLIC4 regulates TGF-beta-dependent myofibroblast differentiation to produce a cancer stroma. *Oncogene* **33**, 842-850 (2014).
40. Glasser, S.W. *et al.* Mechanisms of Lung Fibrosis Resolution. *Am J Pathol* **186**, 1066-1077 (2016).
41. Podhorecka, M., Skladanowski, A. & Bozko, P. H2AX Phosphorylation: Its Role in DNA Damage Response and Cancer Therapy. *J Nucleic Acids* **2010** (2010).
42. Son, Y. *et al.* Mitogen-Activated Protein Kinases and Reactive Oxygen Species: How Can ROS Activate MAPK Pathways? *J Signal Transduct* **2011**, 792639 (2011).
43. Grab, J. & Rybniker, J. The Expanding Role of p38 Mitogen-Activated Protein Kinase in Programmed Host Cell Death. *Microbiol Insights* **12**, 1178636119864594 (2019).
44. Brune, B. Nitric oxide: NO apoptosis or turning it ON? *Cell Death Differ* **10**, 864-869 (2003).
45. Fujii, J., Homma, T. & Osaki, T. Superoxide Radicals in the Execution of Cell Death. *Antioxidants (Basel)* **11** (2022).
46. Zheng, X. *et al.* Redirecting tumor-associated macrophages to become tumoricidal effectors as a novel strategy for cancer therapy. *Oncotarget* (2017).
47. Jiang, H., Hegde, S. & DeNardo, D.G. Tumor-associated fibrosis as a regulator of tumor immunity and response to immunotherapy. *Cancer Immunol Immunother* (2017).
48. Panigrahy, D. *et al.* Preoperative stimulation of resolution and inflammation blockade eradicates micrometastases. *J Clin Invest* **129**, 2964-2979 (2019).
49. Kaplan, R.N., Rafii, S. & Lyden, D. Preparing the "soil": the premetastatic niche. *Cancer Res* **66**, 11089-11093 (2006).

50. Erler, J.T. *et al.* Hypoxia-induced lysyl oxidase is a critical mediator of bone marrow cell recruitment to form the premetastatic niche. *Cancer Cell* **15**, 35-44 (2009).
51. Wong, C.C. *et al.* Hypoxia-inducible factor 1 is a master regulator of breast cancer metastatic niche formation. *Proc Natl Acad Sci U S A* **108**, 16369-16374 (2011).
52. Cox, T.R. *et al.* LOX-mediated collagen crosslinking is responsible for fibrosis-enhanced metastasis. *Cancer Res* **73**, 1721-1732 (2013).
53. Gao, H. *et al.* Multi-organ Site Metastatic Reactivation Mediated by Non-canonical Discoidin Domain Receptor 1 Signaling. *Cell* **166**, 47-62 (2016).
54. Loeffler, M., Kruger, J.A., Niethammer, A.G. & Reisfeld, R.A. Targeting tumor-associated fibroblasts improves cancer chemotherapy by increasing intratumoral drug uptake. *J Clin Invest* **116**, 1955-1962 (2006).
55. Takai, K., Le, A., Weaver, V.M. & Werb, Z. Targeting the cancer-associated fibroblasts as a treatment in triple-negative breast cancer. *Oncotarget* **7**, 82889-82901 (2016).
56. Darby, I.A. & Hewitson, T.D. Fibroblast differentiation in wound healing and fibrosis. *Int Rev Cytol* **257**, 143-179 (2007).
57. Popov, Y. *et al.* Macrophage-mediated phagocytosis of apoptotic cholangiocytes contributes to reversal of experimental biliary fibrosis. *Am J Physiol Gastrointest Liver Physiol* **298**, G323-334 (2010).
58. Zhang, J. & Bowden, G.T. Activation of p38 MAP kinase and JNK pathways by UVA irradiation. *Photochem Photobiol Sci* **11**, 54-61 (2012).
59. Faust, D. *et al.* Differential p38-dependent signalling in response to cellular stress and mitogenic stimulation in fibroblasts. *Cell Commun Signal* **10**, 6 (2012).
60. Redza-Dutordoir, M. & Averill-Bates, D.A. Activation of apoptosis signalling pathways by reactive oxygen species. *Biochim Biophys Acta* **1863**, 2977-2992 (2016).
61. Liu, R.M. & Gaston Pravia, K.A. Oxidative stress and glutathione in TGF-beta-mediated fibrogenesis. *Free Radic Biol Med* **48**, 1-15 (2010).
62. Hecker, L. *et al.* NADPH oxidase-4 mediates myofibroblast activation and fibrogenic responses to lung injury. *Nat Med* **15**, 1077-1081 (2009).
63. Sugiura, H. *et al.* N-acetyl-L-cysteine inhibits TGF-beta1-induced profibrotic responses in fibroblasts. *Pulm Pharmacol Ther* **22**, 487-491 (2009).
64. Hinz, B. & Lagares, D. Evasion of apoptosis by myofibroblasts: a hallmark of fibrotic diseases. *Nat Rev Rheumatol* **16**, 11-31 (2020).
65. Perez, D.A. *et al.* Switching off key signaling survival molecules to switch on the resolution of inflammation. *Mediators Inflamm* **2014**, 829851 (2014).
66. Puente-Cobacho, B., Varela-Lopez, A., Quiles, J.L. & Vera-Ramirez, L. Involvement of redox signalling in tumour cell dormancy and metastasis. *Cancer Metastasis Rev* **42**, 49-85 (2023).
67. Vera-Ramirez, L., Vodnala, S.K., Nini, R., Hunter, K.W. & Green, J.E. Autophagy promotes the survival of dormant breast cancer cells and metastatic tumour recurrence. *Nat Commun* **9**, 1944 (2018).
68. Crist, S.B. *et al.* Unchecked oxidative stress in skeletal muscle prevents outgrowth of disseminated tumour cells. *Nat Cell Biol* **24**, 538-553 (2022).
69. Piskounova, E. *et al.* Oxidative stress inhibits distant metastasis by human melanoma cells. *Nature* **527**, 186-191 (2015).
70. Jain, K., Verma, P.J. & Liu, J. Isolation and handling of mouse embryonic fibroblasts. *Methods Mol Biol* **1194**, 247-252 (2014).
71. Dong, J. & Ma, Q. Osteopontin enhances multi-walled carbon nanotube-triggered lung fibrosis by promoting TGF-beta1 activation and myofibroblast differentiation. *Part Fibre Toxicol* **14**, 18 (2017).
72. Weidenfeld, K. *et al.* Dormant tumor cells expressing LOXL2 acquire a stem-like phenotype mediating their transition to proliferative growth. *Oncotarget* **7**, 71362-71377 (2016).

73. Wegner, K.A., Keikhosravi, A., Eliceiri, K.W. & Vezina, C.M. Fluorescence of Picrosirius Red Multiplexed With Immunohistochemistry for the Quantitative Assessment of Collagen in Tissue Sections. *J Histochem Cytochem* **65**, 479-490 (2017).

Acknowledgments

We would like to thank Shany Barkan for preparing the schemes and reviewing the manuscript. Prof. Pnina Brodt for reviewing the manuscript. We thank Dr. Boris Shklyar, head of the Bioimaging Unit. This work was supported by the British and Swiss Friends of University of Haifa Funds, Israel Science Foundation Grants No. 942/20, Israel Cancer Association grant number 20230084 (To DB), and ResCure Pharma LTD (to DB and AA).

Author contributions

OG, KW, HS, SM, YF, SS, SB designed and or performed experiments and analyzed the data. SA provided technical assistance. PV wrote the macro-program for the 3D image analysis. AS carried out the histological analysis. AA conceived the project. DB conceived, supervised the project and wrote the manuscript.

Competing interests

The research was partly supported by ResCure Pharma until 2017. DB and AA served as scientific consultants at ResCure Pharma until 2017. YF was the scientific manager at ResCure Pharma until 2017. Patent application covering part of the manuscript was awarded : Barkan D, Gilon O, Schif-Zuck S and Ariel A. CD11b^{low} macrophages and conditioned media thereof for treating cancer and /or fibrosis. Patent application No. WO2014102799A1 https://patents.google.com/patent/WO2014102799A1/en.

DB is a scientific consultant to VuJaDe Sciences.

Figures

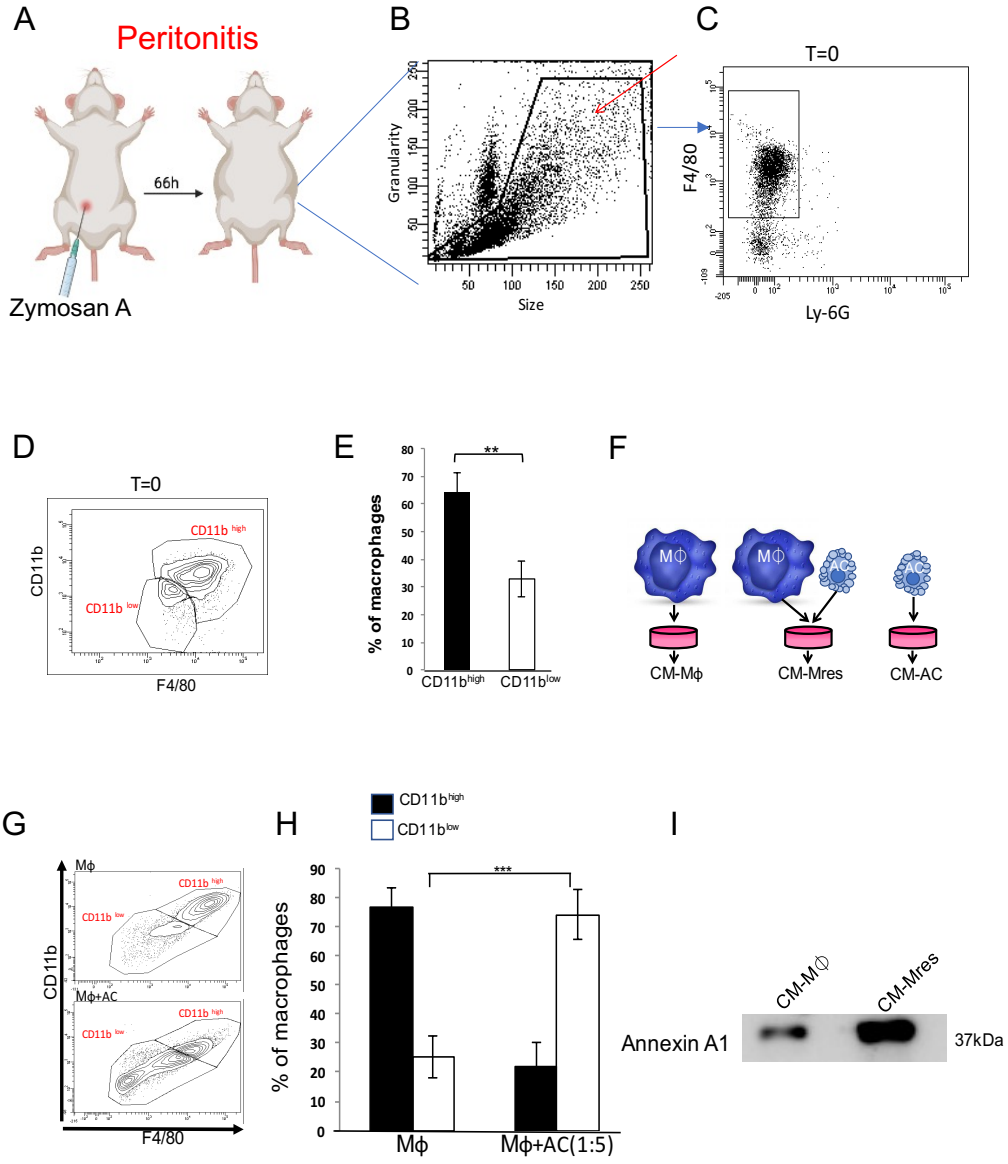

Figure 1: Generation of conditioned media from pro-resolving CD11b^{low}-enriched macrophages; CM-Mres. A-C) Mice were injected I.P. with zymosan A (1 mg/mouse, A) and their peritoneal exudates were collected at 66 hrs. **B)** Gating of exudate macrophages based on their size and granularity**. C)** Histogram of identified macrophages, stained positive for F4/80 and negative for Ly-6G. **D)** Characterization of CD11b expression by F4/80^{+} macrophages. Representative results. **E)** Percentage of CD11b^{high} and CD11b^{low} macrophages before incubation with apoptotic cells (AC). Columns; mean, bars; SEM, n=3. **F)** Illustrative scheme demonstrating the preparation of condition media from peritoneal cells enriched either with CD11b^{high} Mφ (CM- Mφ) or CD11b^{low} Mφ (CM-Mres) or from control unengulfed AC (CM-AC). **G-H)** To verify conversion of CD11b^{high} to CD11b^{low} Mφ upon engulfment of AC, cell samples were stained as above and analyzed by flow cytometry; contour plots (G) and averages (H). Representative results (n=3). Columns; mean, bars; SEM, ** p≤0.01; *** P<0.001. **I)** Representative western blot (W.B) analysis (n=3) of Annexin A1 levels in CM- Mφ and CM-Mres.

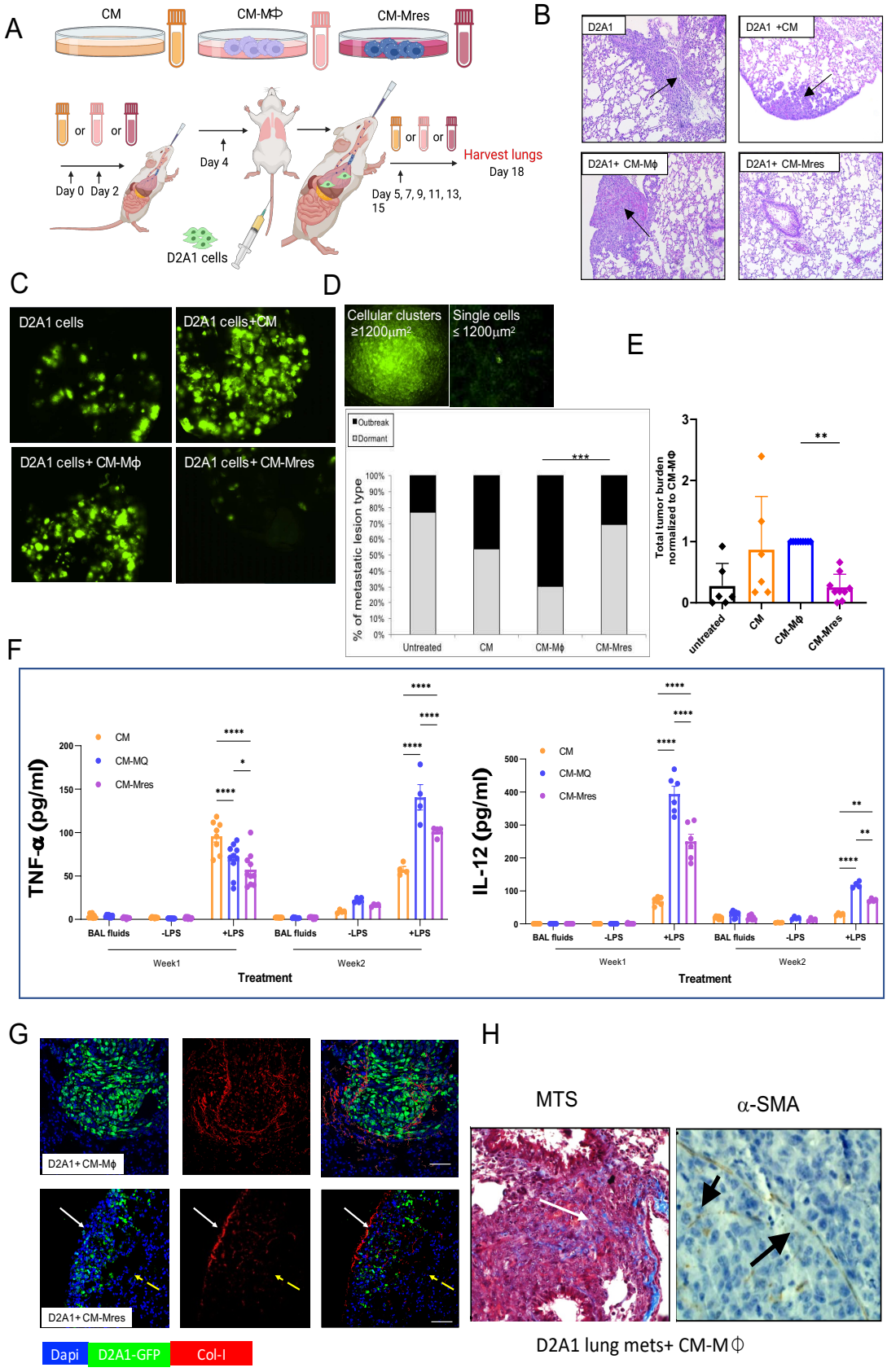

Figure. 2: CM-Mres prevents the metastatic outgrowth of dormant D2A1-GFP cells *in vivo*. A) An illustrative scheme of the experimental regimen of D2A1-GFP lung metastasis with conditioned media treatment. **B-F)** Mice were tail-vein injected with either $0.5x10^6$ (B-C) or with $200x10^3$ D2A1-GFP cells/mouse (D-H). After 2 weeks, lungs were harvested and imaged by

SCOM. **B)** Representative paraffin sections (n=3) of lungs colonized with D2A1-GFP cells either untreated (upper left pane) or treated with the different conditioned media. Paraffin sections were subjected to hematoxylin and eosin staining (H&E), black arrow heads denote metastatic lesion. **C)** Representative SCOM images of whole lungs from either untreated (upper left panel) or treated with CM (upper right panel), CM-Mφ (lower left panel) or CM-Mres (lower right panel). Magnification x10, n=3. **D)** Upper panel: Representative images of single cells (foci ≤1200 μm^2) and multi-cellular proliferative metastatic lung lesions (cell clusters >1200 μm^2). Lower panel: Percentage of dormant single cells versus multi-cellular proliferative metastatic lung lesions in mice as depicted in upper panel, n=4-8 mice. **E)** Total D2A1-GFP tumor cell burden /lung. **F)** BAL fluids and alveolar Mφ (AM) were isolated from lungs of mice colonized with D2A1–GFP cells treated either with CM, CM-Mφ or CM-Mres, 1 or 2 weeks post treatment. AM were activated with LPS (1μg/ml) and evaluated for secretion of cytokines using standard ELISA. n=4-8 mice; Columns; mean, bars; SEM, * $p \leq 0.05$, ** $p \leq 0.01$, **** $p \leq 0.001$. **G)** Two sequential paraffin sections of lungs colonized with D2A1-GFP cells treated either with CM-Mφ or CM-Mres were stained either with picrosirius-red (RED) to detect Col-I bundles (see white arrow) or immunostained with antibody to detect GFP expressing cells (green). Yellow arrow denotes area in the lung with no tumor and no Col-I staining. Sections were counterstained with DAPI to detect nuclei (blue). Confocal Images. Magnification x60, scale bar=50μm. **H)** Paraffin sections of lungs with D2A1-GFP lesion treated with CM- Mφ. Left panel: stained for Col-I expression by MTS (blue) (see white arrow). Right panel: stained for cells expressing α-SMA (brown) and nuclei counterstained with hematoxylin (blue).

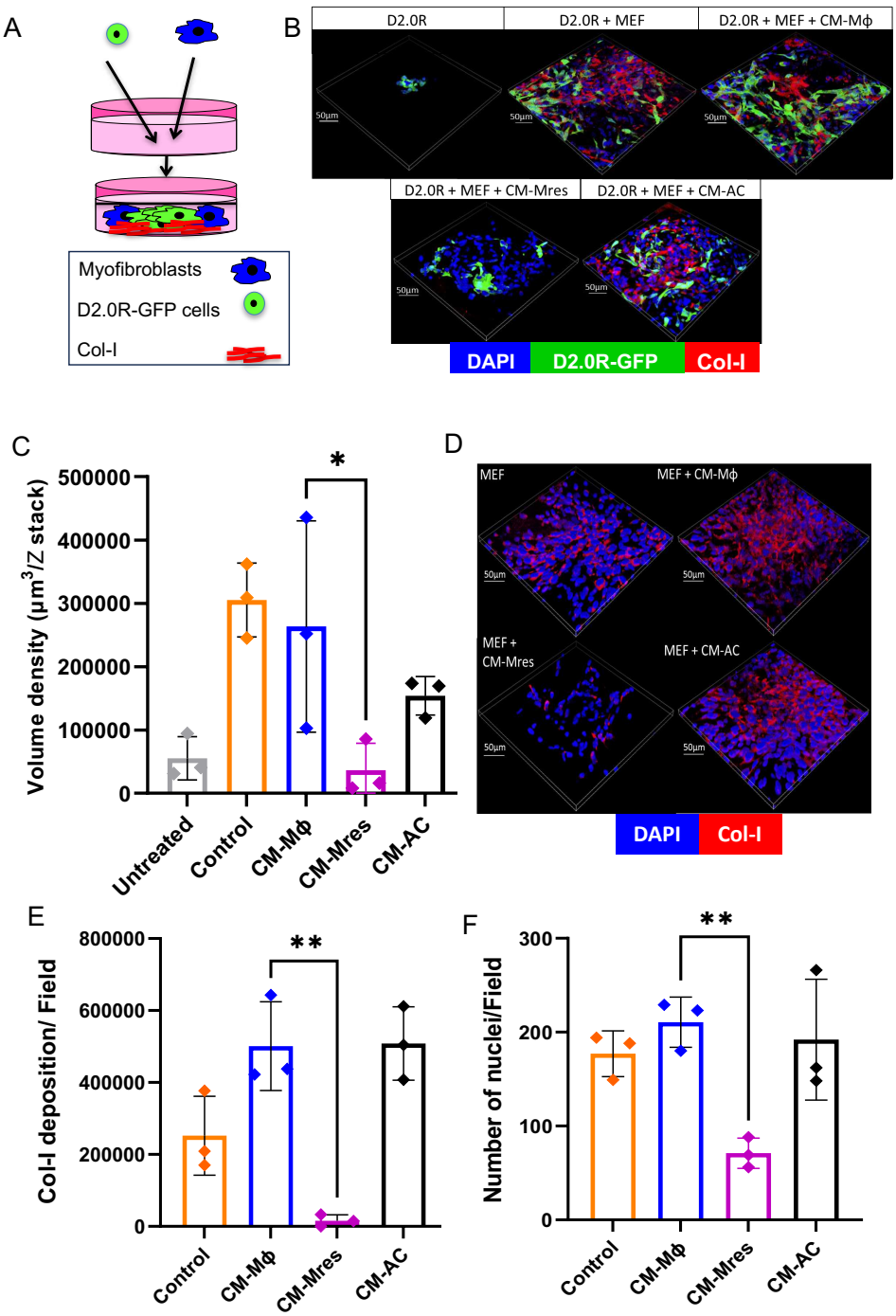

Figure. 3: CM-Mres prevents the metastatic outbreak of dormant tumor cells co-cultured with myofibroblasts in the 3D BME system. A) An illustrative scheme of D2.0R-GFP cells (green) co-cultured in the 3D BME system with MEF. Nuclei staining with DAPI (blue) and immunofluorescence staining for Col-I (red). **B)** Representative confocal images of Z-stack of the co-culture system. Magnification x40. Bars=50µm. **C)** Quantification of the number of D2.0R-GFP cells in (B), representative results, n=3. **D)** Representative images (n=3) of immunofluorescent staining for Col-I expression (red) of myofibroblasts in the 3D BME system either untreated (upper left pane) or treated with the indicated conditioned media. **E)** Quantification of Col-I expression in (D). **F)** Proliferation of myofibroblasts in (D) determined by the number of nuclei in middle section of the Z-stack (DAPI, blue)/field, n=3 fields. Columns; mean, bars; SEM, *p≤0.05, **P≤0.01.

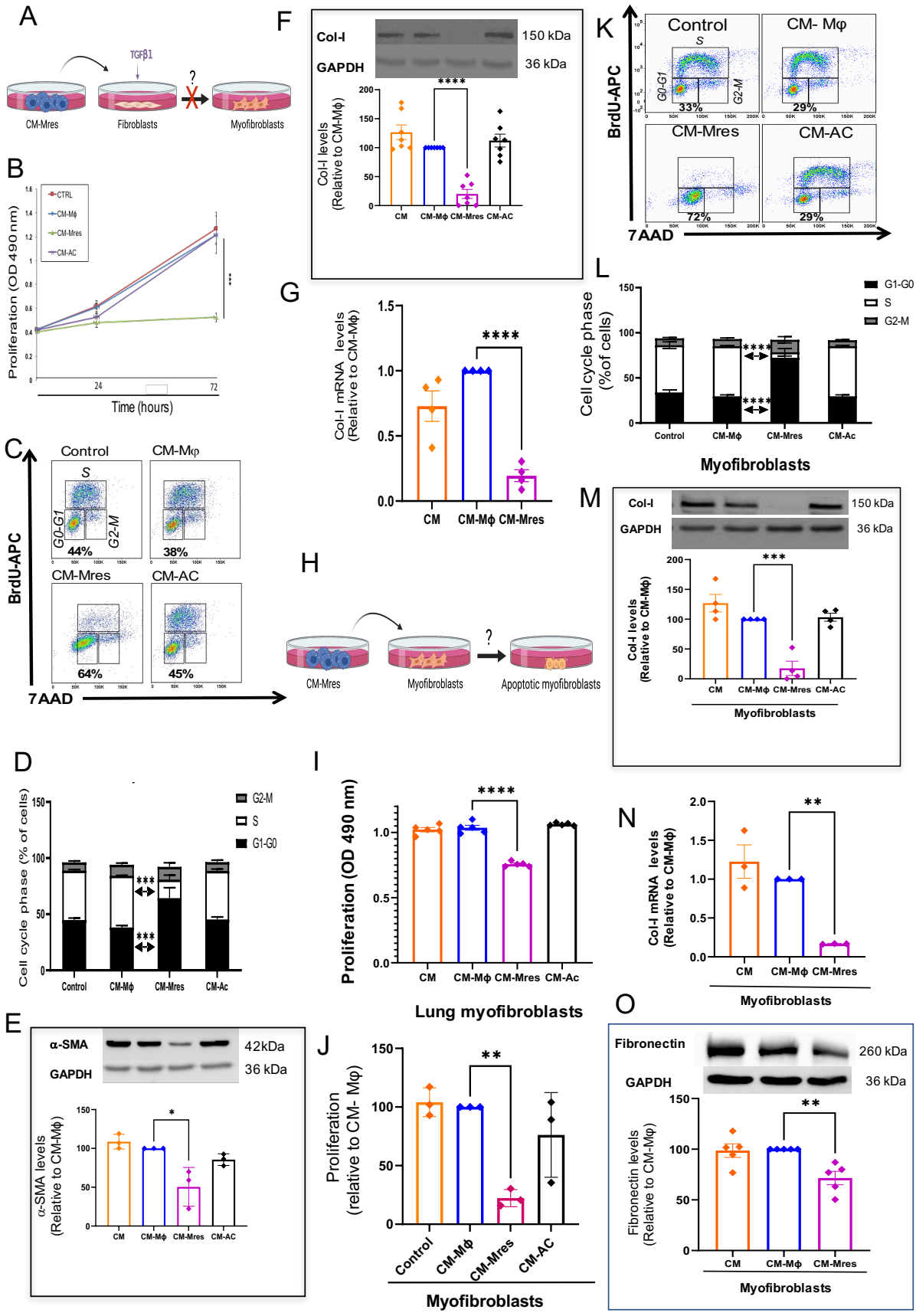

Figure. 4: CM-Mres inhibits fibroblast differentiation to myofibroblasts and inactivates myofibroblasts. A-G) Starved MEF were cultured in 2D culture and pretreated with either CM, CM-Mφ, CM-Mres or CM-AC. 2hrs later the cells were treated with TGFβ1 (1ng/ml) for additional 72h. **A)** Experimental scheme**. B)** Proliferation of MEF cells. Points; mean (n=5 replicates), bars;

SEM. Representative result, n=3. **C)** Representative dot blots of the FACS analysis of cell cycle, determined by BrdU incorporation**. D)** Quantification of the percentage of cells at G0-G1, S and G2-M phase. n=2. **E)** Representative W.B. of α-SMA expression by differentiating MEF (upper panel) and α-SMA quantification (lower panel), n=3. **F)** Representative W.B. of Col-I expression by differentiating MEF (upper panel) and Col-I quantification (lower panel). Densitometry values (E-F) were normalized to TGFβ1 treated MEF with CM-Mφ, n=7. **G)** qPCR of Col-I mRNA levels; values were normalized to GAPDH, n=4. **H-O)** Myofibroblasts were treated with the different conditioned media. **H)** Experimental scheme. **I-J)** Proliferation of myofibroblasts derived either from lung fibroblasts (representative result, n=2) (I) or from MEF (J) (n=3) treated with CM-Mφ, CM-Mres or CM-AC. Columns; mean, bars; SEM, n=5 replicates. **K)** Representative dot blots of the cell cycle analysis of myofibroblasts derived from MEF. Cell cycle determined by BrdU incorporation. **L)** Quantification of the percentage of cells in (K) at G0-G1, S and G2-M phase, n=3. **M)** Upper panel: Representative W.B. of Col-I expression by myofibroblasts derived from MEF. Lower panel: Col-I quantification. Densitometry values were normalized to myofibroblasts treated with CM-Mφ, n=4. **N)** qPCR of the mRNA levels of Col-I, n=3. **O)** Upper panel: Representative W.B. of fibronectin expression by myofibroblasts derived from MEF. Lower panel: fibronectin quantification. Densitometry values were normalized to myofibroblasts treated with CM-Mφ. Columns; mean, bars; SEM, n=5. **P≤0.01; *** P≤0.001, ****p≤0.0001.

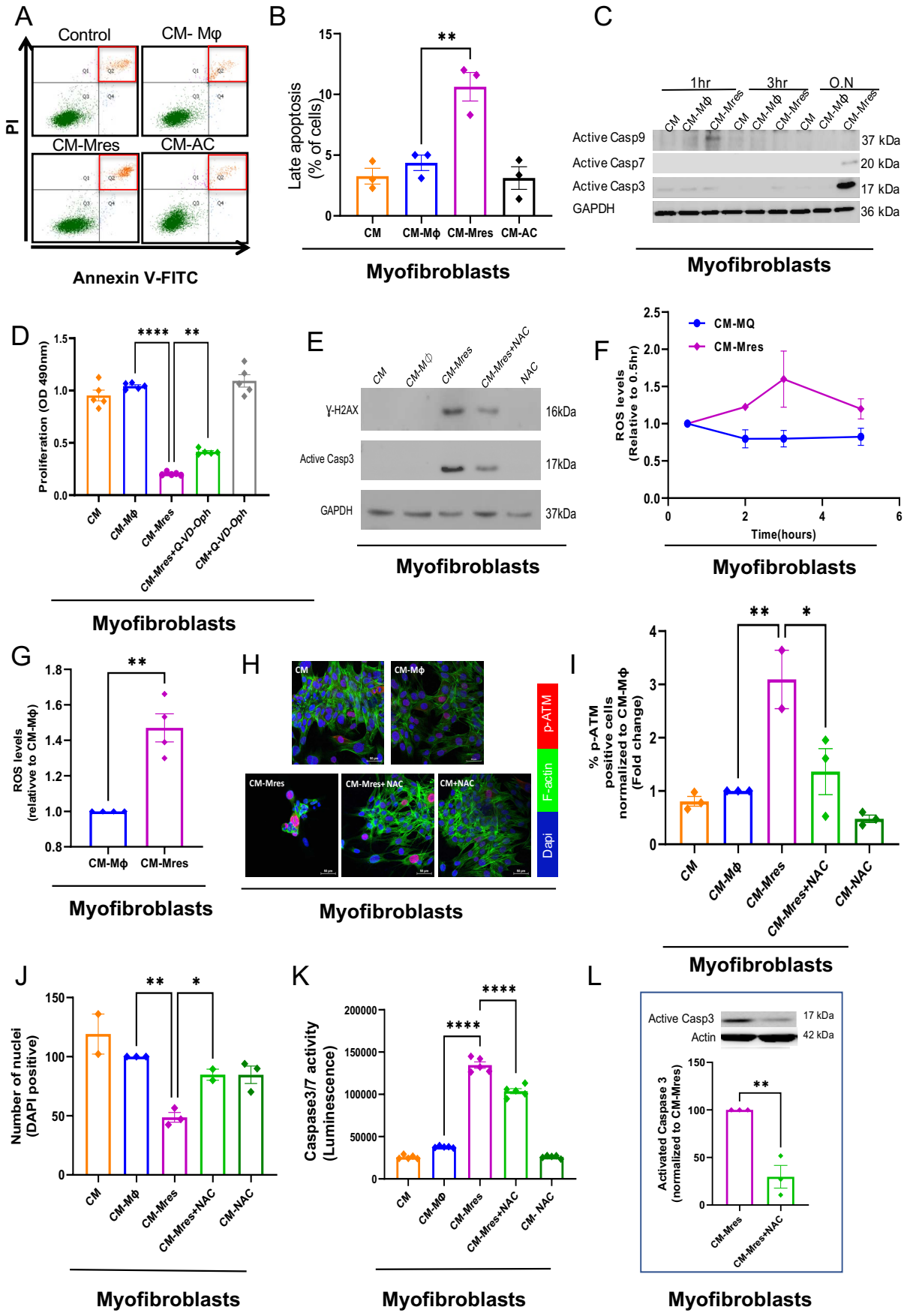

Figure. 5: CM-Mres promotes an increase in ROS levels in myofibroblasts resulting in DNA damage and apoptosis. A) Representative dot plots of Annexin V and PI staining of myofibroblasts treated with the different conditioned media for 6h. Red square; percentage of cells displaying late

apoptosis, n=3. **B)** Quantification of the percentage of cells stained positive for Annexin V and PI staining. **C)** W.B. analysis of the expression levels of activated caspase 9/7/3 in myofibroblasts treated with different conditioned media for 1h, 3h or O.N. **D)** Proliferation of myofibroblasts treated with either CM or CM-Mres in the absence or presence of caspase inhibitor Q-VD-Oph (20 μM) or with CM-Mφ for 72h. Representative graph, Columns; mean (5 replicates), bars; SEM, n=5. **E)** W.B. analysis of γH2AX expression in myofibroblasts treated with either CM or CM-Mres in the absence or presence of NAC (10 μM) or with CM-Mφ for 24h. **F)** Time course of ROS levels (determined by MFI of DCFDA) in myofibroblasts treated either with CM-Mφ or CM-Mres, for 0.5h, 2h, 3h or 5h. **G)** Quantification of ROS levels in myofibroblasts treated either with CM-Mφ or CM-Mres for 3h. MFI values were normalized to myofibroblasts treated with CM-Mφ, n=4. **H-J)** Myofibroblasts were either treated with CM, CM-Mφ, CM-Mres, CM-Mres+NAC (10 mM) or CM+NAC for 24h. **H)** Representative confocal images of middle cross section of myofiboblasts stained for p-ATM (red), nuclei (DAPI, blue) and F-actin (green). Magnification x40, Bars =50μm. **I)** Quantification of the percentage of p-ATM positive cells /acquired $2mm^2$ field (tiling 5x5). The percentage of p-ATM were normalized to myofibroblasts treated with CM-Mφ. **J)** Quantification of the number of nuclei (DAPI positive cells)/ acquired $2mm^2$ field. Number of nuclei were normalized to myofibroblasts treated with CM-Mφ. Columns; mean (n=3 fields), bars; SEM, n=2. **K)** Caspase3/7 activity in myofibroblasts treated with either CM or CM-Mres in the absence or presence of NAC (10 mM) or with CM-Mφ for 24. Representative graph. Columns; mean (5 replicates), bars; SEM, n=5. **L)** Upper panel: Representative W.B analysis of activated Caspase- 3 expression in myofibroblasts treated with CM-Mres in the absence or presence of NAC (10mM). Lower panel: activated Caspase3 quantification. Densitometry values were normalized to myofibroblasts treated with CM-Mres. Columns; mean, bars; SEM, n=3. * $P \leq 0.05$; ** $P \leq 0.05$, **** $P \leq 0.0001$.

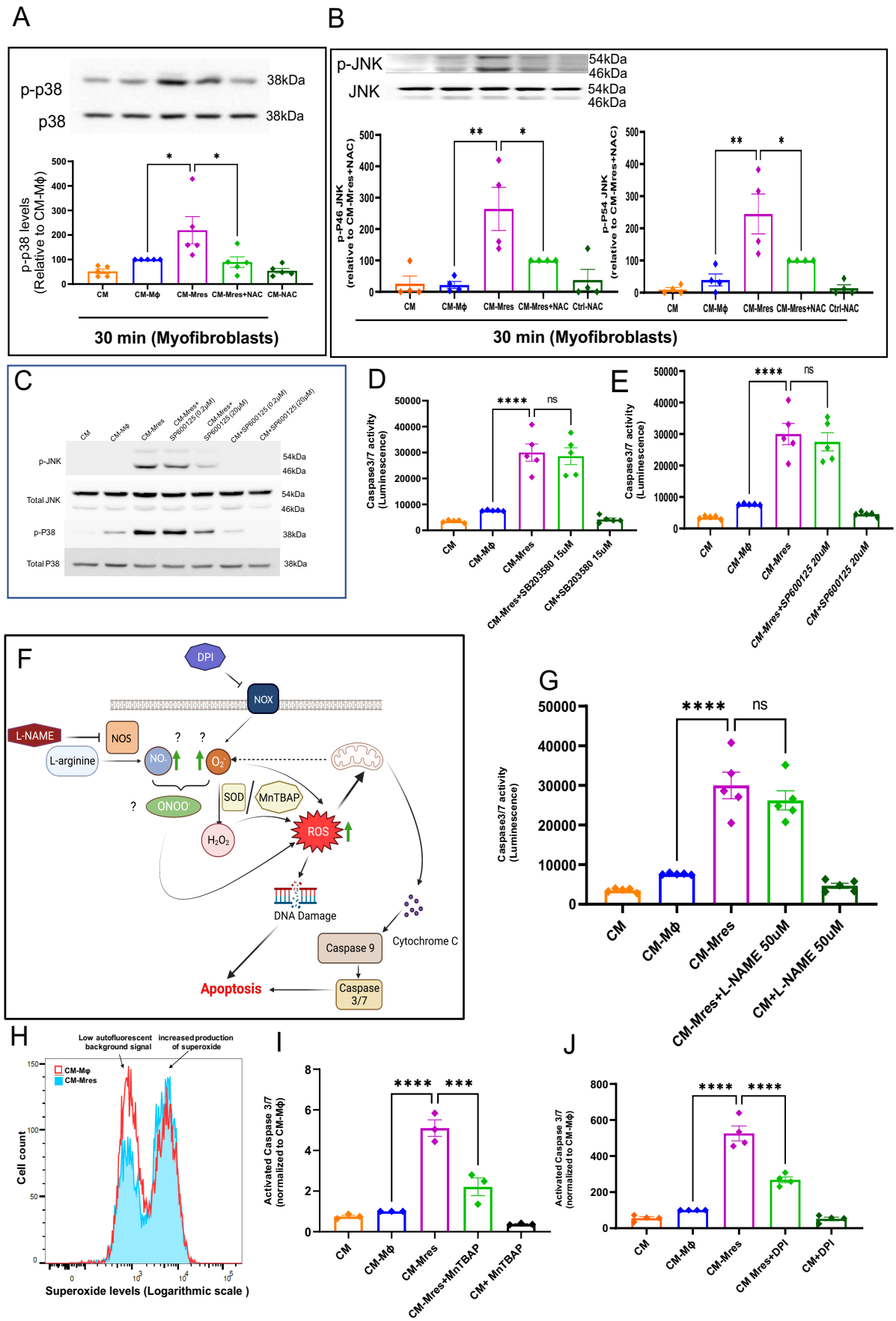

Fig. 6: CM-Mres promotes oxidative stress in myofibroblasts by increasing superoxide levels via NADPH oxidase. A-B) Myofibroblasts were treated with either CM or CM-Mres in the absence or presence of NAC (10 mM) or with CM-Mφ for 30 min **A)** Upper panel: Representative W.B. analysis of phospho-p38 (p-p38) after 30 min. Lower panel: p-p38 quantification. **B)** Upper panel:

Representative western blot analysis of phospho-JNK (p-JNK). Lower panel: p-JNK quantification. Densitometry values of p-p38 (normalized to p38) and p-JNK (normalized to JNK respectively) are relative to myofibroblasts treated with CM-Mφ+NAC. Columns; mean, bars; SEM, n=4. **C)** W.B analysis of p-JNK and p-p38 expression levels in myofibroblasts treated with CM or CM-Mres in the absence or presence of JNK inhibitor SP600125 (0.2μM, 20μM) or with CM-Mφ for 30min. **D-E)** Caspase3/7 activity in myofibroblasts treated with CM or CM-Mres in the absence or presence of either SB 203580 (15 μM), SP600125 (20 μM) or with CM-Mφ (D and E respectively) for 24h. Columns; mean (n= 5 replicates), bars; SEM. **F)** A scheme demonstrating potential pathways involved in ROS generation. L-NAME; a nitric oxide synthase (NOS) inhibitor, Diphenyleneiodonium chloride (DPI); a pan inhibitor of NADPH oxidase (NOX) and MnTBAP; superoxide dismutase (SOD) mimetic. **G)** Caspase3/7 activity in myofibroblasts treated with CM or CM-Mres in the absence or presence of L-NAME (50 μM) or with CM-Mφ for 24h. Columns; mean (n= 5 replicates), bars; SEM. **H)** Histogram representing superoxide levels (determined by FACS analysis) in myofibroblasts treated with either CM-Mφ or CM-Mres for 15 min. **I-J)** Caspase3/7 activity in myofibroblasts treated with CM or CM-Mres in the absence or presence of either MnTBAP (100 μM) (I), DPI (0.1 μM) (J) or with CM-Mφ for 24h. Data was normalized to CM- Mφ. Columns; mean, bars; SEM. n=3-4. * $P \leq 0.05$; ** $P \leq 0.05$, *** $P \leq 0.001$, *** $P \leq 0.0001$.

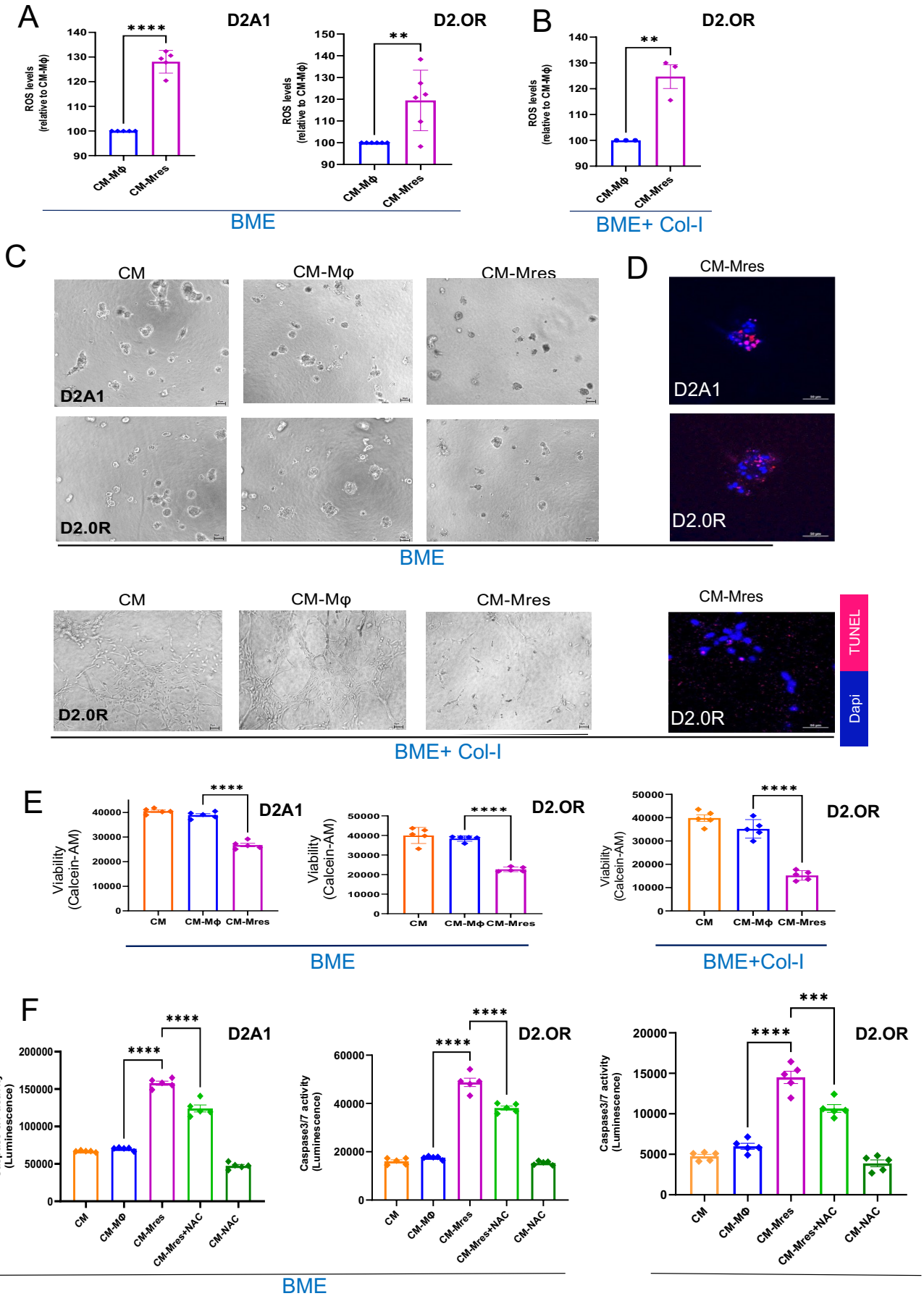

Figure. 7: CM-Mres promotes apoptosis of dormant and outbreaking mammary cancer cells in the 3D BME system via induction of ROS. A-D) Dormant D2A1 (n=4) and dormant D2.0R cells (n=6) cultured for 72h in the 3D BME system (A) and outbreaking D2.0R cells (n=3) cultured in the

3D BME supplemented with Col-I (BME+Col-I) (B). A-B) the above cells were treated with either CM-Mφ or CM-Mres. For 1h and ROS levels were determined. Values were normalized to treatment with CM-Mφ. **C)** Representative light microscopy images of dormant D2A1 and D2.0R cells in the 3D BME system and of outbreaking D2.0R cells in the 3D BME+Col-I system treated with CM-Mres for 24h. Magnification x10, Bars =50μm. **D)** Representative confocal image of TUNEL staining of dormant D2A1, D2.0R cells in the 3D BME system and of outbreaking D2.0R cells in the 3D BME+ Col-I system upon treatment with CM-Mres for 24h. **E)** Viability of dormant D2A1 and D2.0R cells in the 3D BME system and of outbreaking D2.0R cells in the 3D BME+Col-I system was determined 72h post treatment by Calcein-AM staining. n=5. **F)** Caspase3/7 activity in dormant D2A1 and D2.0R cells in the 3D BME system and in outbreaking D2.0R cells cultured in the 3D BME+ Col-I system that were treated either with CM or CM-Mres in the absence or presence of NAC (10 mM) or with CM-Mφ for 24h. Representative graph (n=3). Columns; mean (5 replicates), bars; SEM. ** $P \leq 0.05$, *** $P \leq 0.001$, **** $P \leq 0.0001$.

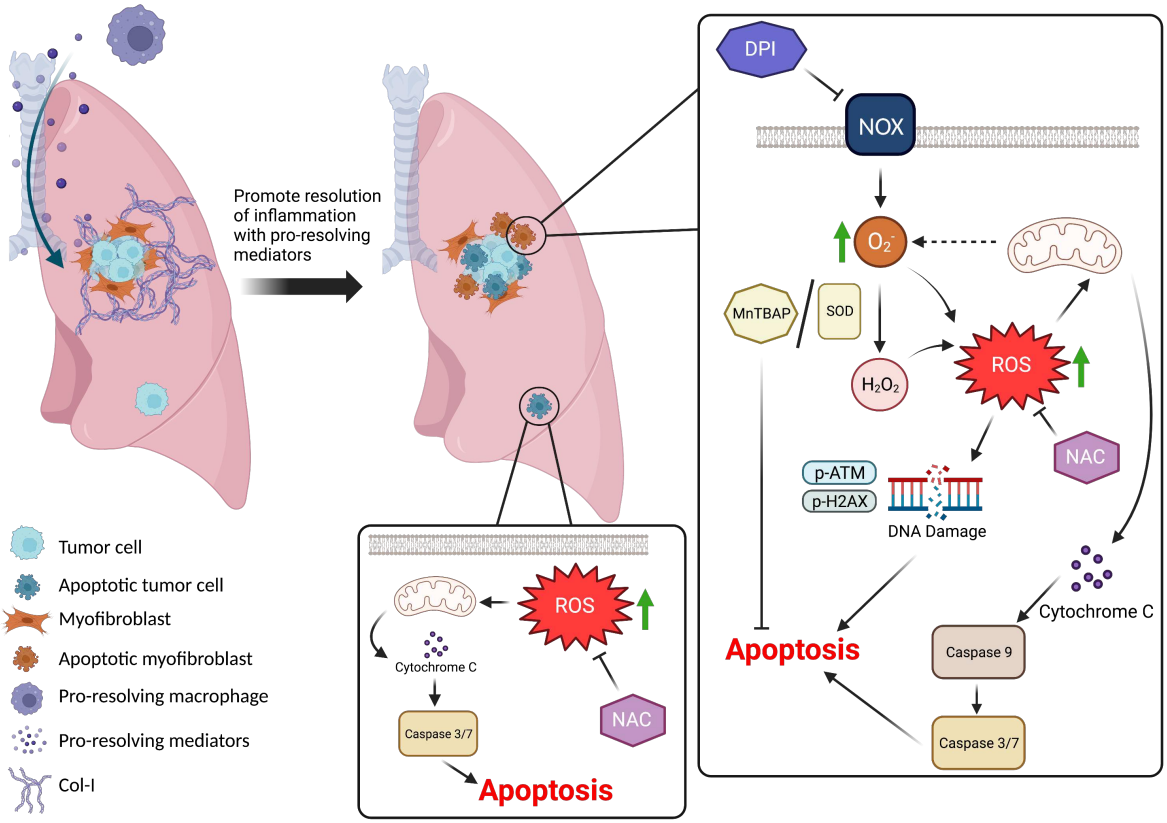

Figure. 8: Proposed mechanism by which macrophage-derived pro-resolving mediators prevent metastatic outgrowth of dormant DTCs. Promoting resolution of inflammation by CM-Mres prevents the formation of Col-I enriched fibrotic-like milieu by inhibiting fibroblasts differentiation to myofibroblasts and promoting myofibroblasts apoptosis. Apoptosis is induced upon an increase in O_2^- levels via NOX. This in turn increases ROS levels culminating in DNA damage (DSB); depicted by an increase in p-ATM and p-H2AX(γ-H2AX) and activation of caspase 9 and its downstream effector caspases 7/3 leading to apoptosis. This proposed mechanism is supported in part by the observation that upon treatment with either NAC (ROS scavenger), DPI (inhibitor of NOX), or treatment with SOD mimetics (MnTBP), apoptosis was inhibited. In addition, CM-Mres induced apoptosis in dormant DTCs and in DTCs emerging form their dormant state by inducing oxidative stress via elevated ROS levels and activation of caspase3/7, while in the presence of NAC apoptosis was inhibited.

Supplementary Files

This is a list of supplementary files associated with this preprint. Click to download.

- GilonOetalSupplementaryFigures.pdf